

Microwave Response of Superconductors with Paramagnetic Impurities

Mehdi Zarea* and J. A. Sauls†

Hearne Institute of Theoretical Physics, Louisiana State University, Baton Rouge LA 70803 USA

(Dated: December 24, 2025)

We develop theoretical methods to predict the effects of paramagnetic impurities on the microwave response of conventional spin-singlet superconductors. Our focus is on superconducting devices and resonators with *low concentrations* of impurities and *exchange interactions* with conduction electrons. We connect the sub-gap quasiparticle spectrum generated by pair-breaking to the frequency and temperature dependence of the conductivity for superconductors operating at microwave frequencies. We report theoretical results for superconducting device performance - dissipation, quality factor and frequency shift anomalies - based on self-consistent calculations of the current response and penetration of the electromagnetic field at the vacuum-superconducting interface. Key results include the prediction of a non-monotonic anomaly in the low-frequency superfluid fraction and penetration depth at very low temperatures related to the sub-gap quasiparticle spectrum. Dissipation of microwave power is predicted from intra- and inter- impurity band transitions at GHz frequencies at low temperatures, including a physical mechanism responsible for residual resistance. We predict anomalies in the resonant frequency, $f(T)$, and quality factor, $Q(T)$, of high-Q SRF cavities operating in the GHz range at low-temperatures that are sensitive to non-magnetic and paramagnetic impurity disorder.

I. INTRODUCTION

A known source of decoherence for superconducting resonators and qubits is dissipation from quasiparticles under nonequilibrium conditions. Indeed quasiparticle dissipation is reported to be as important as all other loss channels in transmon qubits when coherence times exceed $200 \mu\text{sec}$ [1]. Potential sources of a significant population of quasiparticles leading to decoherence in superconducting devices range from high current densities and multi-photon pair breaking [2, 3], energy deposition from background radiation and cosmic rays [4, 5], to sub-gap of Andreev bound states generated by surface defects [6] or pair-breaking by TLS impurities [7].

The effects of impurity disorder on superconductivity was studied extensively soon after the development of the microscopic theory of superconductivity [8] by many authors [9–12]. For recent studies related to microwave resonators and SRF cavities see Refs. [13–17]. In this report we focus on the role and impact of dilute concentrations of paramagnetic impurities on the microwave response of superconducting circuits and resonators.

A. Background

The exchange coupling of electrons to paramagnetic impurities is well known to break Cooper pairs, leading to unpaired quasiparticle states below the continuum threshold (“gap edge”) of quasiparticle excitations. Abrikosov and Gorkov (AG) [11] were first to study the effects of randomly distributed paramagnetic impurities on the properties of conventional superconductors. The electron-impurity exchange interaction, $J\vec{S}\cdot\vec{s}$, was treated perturbatively in the Born approximation, with $\vec{s} = (\hbar/2)\vec{\sigma}$ the electron spin operator, $\vec{\sigma}$ are the Pauli matrices and \vec{S} is the impurity spin. AG calculated the suppression of the transition temperature T_c , and the mean-field superconducting order parameter (“gap” function), $\Delta(T)$, as a function of the Born scattering rate, $1/\tau_S = \pi N_f J^2 S(S+1)$. They also showed that for increasing impurity concentration *gapless superconductivity* is possible, i.e. a range of impurity concentrations for which there

is a finite density of states down to the Fermi level, yet T_c and Δ are finite, see also Ref. 18.

The effects of spin-exchange scattering beyond the Born approximation were pioneered by Yu [19], Shiba [20] and Rusinov [21] (YRS). These authors included the exchange interaction to all orders in the amplitude for quasiparticles, including those forming Cooper pairs, scattering off the impurity spin, the latter treated as a classical spin. For an isolated paramagnetic impurity, exchange scattering generates quasiparticle states with energies below the continuum edge, $\pm\varepsilon_l = \pm\Delta \cos(\delta_l^+ - \delta_l^-)$, where δ_l^\pm are the phase shifts for quasiparticles with orbital angular momentum l relative to the impurity with spin aligned parallel (+) or anti-parallel (–) to that of the impurity spin [21]. Note that there are impurity states with excitation energy above the Fermi level (particle-like), $0 \leq +\varepsilon_l < \Delta$, and impurity states below the Fermi energy, $-\Delta < -\varepsilon_l \leq 0$. The negative energy states are occupied for the $T = 0$ ground state; thus, hole-like excitations are created at finite temperature and under the action of electromagnetic (EM) fields. For a finite concentration of randomly distributed impurities the spectrum broadens into an *impurity band*, with bandwidth determined by the impurity concentration, and the center of the band determined primarily by the strength of the exchange interaction [20, 22].

B. Outline

We begin with theoretical methods in Sec. II based on the quasiclassical theory of superconductivity [23–25], combined with configurational-averaged scattering theory of quasiparticles, including bound pairs, by random distributions of non-magnetic and paramagnetic impurities [7, 11, 26]. Our formalism, and notation, follows closely that of Ref. 27. Section II C includes the formulation and development of the T-matrix and self energies for scattering by both non-magnetic and paramagnetic impurities.

These methods are used to calculate the pair-breaking effects of impurities on both equilibrium and nonequilibrium properties of conventional spin-singlet superconductors reported in Secs. II C 4 and II C 5. Our focus is on superconducting devices and resonators with *low concentrations* of impurities with quasiparticle-impurity exchange interactions.

In Sec. III we connect the sub-gap quasiparticle spectrum to the frequency and temperature dependences of the a.c. conductivity for superconducting elements operating at microwave frequencies. Results for superconducting device

* zarea.mehdi@gmail.com

† sauls@lsu.edu

performance are based on the causal (retarded) current response to a transverse EM field obtained from the nonequilibrium Keldysh propagator. The signature of paramagnetic impurities on the penetration of the microwave field into a superconductor is discussed in Sec. III B. In particular, a non-monotonic anomaly in the superfluid fraction at low temperatures is related to the sub-gap spectrum of quasiparticles generated by scattering from paramagnetic impurities.

Section III C includes our results for dissipation at microwave frequencies obtained from the current response of the low-energy band of sub-gap quasiparticles. In particular, we find that dissipation arises from both intra-band transitions at low temperatures, $\hbar\omega \in \varepsilon_{\text{imp}} \ll \Delta$, where ε_{imp} is the impurity band, as well as inter-band transitions between a nearly occupied negative energy band, $-\varepsilon_{\text{imp}}$, and a nearly unoccupied positive energy band, $+\varepsilon_{\text{imp}}$.

In Sec. III D we report results for the impact of paramagnetic impurities on the resonance frequency, $\delta f(T)$, and quality factor, $Q(T)$, for high-Q superconducting resonators operating in the GHz range at low-temperatures. Quasiparticle scattering by paramagnetic impurities effects the resonant frequency shift of the cavity for temperatures close to T_c . The width and depth of the anomalous (negative) frequency shift in Nb-based SRF cavities [15, 16, 28] is impacted by exchange scattering from paramagnetic impurities. We also show that a low-energy sub-gap spectrum of quasiparticles leads to a *residual surface resistance*, $R_s(0)$, and thus a limiting value of Q in good agreement with experimental results on Nb SRF cavities after removal of surface oxides [29].

Readers not interested in theoretical methods can jump to Sec. II C 4.

II. THEORETICAL METHODS

The quasiclassical theory of superconductivity formulated by Eilenberger [23] and Larkin and Ovchinnikov [24] is ideally suited for computational studies of nonequilibrium response of superconductors to electromagnetic fields. The central elements of the theory are the propagators and self energies obtained by quasiclassical reduction of the field theoretical formulation of the theory of superconductivity [30, 31], c.f. Ref. 27.

The quasiclassical propagators - Matsubara, retarded, advanced and Keldysh ($x = \{M, R, A, K\}$) - are functions of the phase-space variables, $(\mathbf{r}, \mathbf{p}_f)$, where \mathbf{r} is the position in coordinate space and \mathbf{p}_f is the position *on the Fermi surface*, i.e. the Fermi momentum¹,

$$\widehat{\mathcal{G}}^x(\mathbf{p}, \mathbf{r}; \varepsilon, t) \equiv \frac{1}{a} \int d\xi_{\mathbf{p}} \widehat{\tau}_3 \widehat{G}^x(\mathbf{p}, \mathbf{r}; \varepsilon, t), \quad (1)$$

where $0 < a < 1$ is the spectral weight of the normal-state quasiparticle pole centered at excitation energy $\xi_{\mathbf{p}} = v_f(|\mathbf{p}| - p_f)$ near the Fermi surface, and

$$\widehat{\tau}_1 = \begin{pmatrix} 0 & \hat{1} \\ \hat{1} & 0 \end{pmatrix}, \widehat{\tau}_2 = \begin{pmatrix} 0 & -i\hat{1} \\ i\hat{1} & 0 \end{pmatrix}, \widehat{\tau}_3 = \begin{pmatrix} \hat{1} & 0 \\ 0 & -\hat{1} \end{pmatrix}, \quad (2)$$

are the diagonal Pauli matrices in particle-hole, ‘‘Nambu’’, space and $\hat{1}$ is the unit matrix in spin space².

Equilibrium states are described by the Matsubara propagator which can be expressed in terms of the quasiparticle and quasihole propagators, the diagonal elements in Nambu space, and the off-diagonal quasiclassical Cooper pair propagators,

$$\widehat{\mathcal{G}}(\mathbf{p}, \mathbf{r}; \varepsilon_n) = \begin{pmatrix} \widehat{g}(\mathbf{p}, \mathbf{r}; \varepsilon_n) & \widehat{f}(\mathbf{p}, \mathbf{r}; \varepsilon_n) \\ \widehat{f}(\mathbf{p}, \mathbf{r}; \varepsilon_n) & \widehat{g}(\mathbf{p}, \mathbf{r}; \varepsilon_n) \end{pmatrix}, \quad (3)$$

where \widehat{g} (\widehat{f}) is the 2×2 spin matrix quasiparticle (pair) propagator for momenta \mathbf{p} on the Fermi surface, Matsubara energy, $\varepsilon_n = (2n+1)\pi/\beta$ where $\beta = 1/T$ and T is the absolute temperature, as a function of position \mathbf{r} ³. The lower components, \widehat{g} and \widehat{f} , define the propagator for hole-like quasiparticles and the conjugate pair propagator, which are related to \widehat{g} and \widehat{f} by Fermion exchange symmetry and particle-hole symmetry⁴.

The equal-time propagator defines the one-particle density matrix in Nambu space,

$$\widehat{\rho}(\mathbf{p}, \mathbf{r}) \equiv \lim_{\tau \rightarrow 0^+} \frac{1}{\beta} \sum_n \widehat{\mathcal{G}}(\mathbf{p}, \mathbf{r}; \varepsilon_n) e^{-i\varepsilon_n \tau / \hbar}, \quad (4)$$

from which all one-body observables can be calculated. For example, the local electron spin density is given by

$$\vec{s}(\mathbf{r}) = N_f \int dS_{\mathbf{p}} \text{Tr} \{ \widehat{\rho}(\mathbf{p}, \mathbf{r}) \widehat{\vec{s}} \}, \quad (5)$$

$$\text{where } \widehat{\vec{s}} \equiv \frac{\hbar}{2} \widehat{\Sigma} = \frac{\hbar}{2} \begin{pmatrix} \vec{\sigma} & 0 \\ 0 & \vec{\sigma}^{\text{tr}} \end{pmatrix}, \quad (6)$$

is the quasiparticle spin operator in Nambu space, with $\vec{\sigma}$ being the 2×2 Pauli spin matrices⁵, and the integration is an average over the Fermi surface.

Similarly, the local equilibrium Cooper pair amplitude is defined by the equal-time limit of Gorkov’s anomalous propagator,

$$\widehat{f}(\mathbf{p}, \mathbf{r}) \equiv \frac{1}{\beta} \lim_{\tau \rightarrow 0^+} \sum_n \widehat{f}(\mathbf{p}, \mathbf{r}; \varepsilon_n) e^{-i\varepsilon_n \tau / \hbar}. \quad (7)$$

Analytic continuation of the diagonal Matsubara propagator to the real energy axis determines the retarded propagator, $\widehat{\mathcal{G}}^R(\mathbf{p}, \mathbf{r}; \varepsilon) = \widehat{\mathcal{G}}(\mathbf{p}, \mathbf{r}; i\varepsilon_n \rightarrow \varepsilon + i0^+)$, from which the spectral resolution of one-body observables are defined. In particular, the spin-averaged, local density of states for quasiparticles with momenta and excitation energies near the Fermi surface is,

$$N(\mathbf{p}, \mathbf{r}; \varepsilon) = -\frac{N_f}{4\pi} \text{Im} \text{Tr} \{ \widehat{\tau}_3 \widehat{\mathcal{G}}^R(\mathbf{p}, \mathbf{r}; \varepsilon) \}. \quad (8)$$

A. Eilenberger’s Equations

The quasiparticle and anomalous pair propagators, organized into 4×4 Nambu matrices, obey Gorkov’s equations [32]. Eilenberger transformed Gorkov’s equations [32] for the quasiparticle and anomalous pair propagators, into

¹ Hereafter we set $\mathbf{p}_f \rightarrow \mathbf{p}$ for momenta on the Fermi surface, and omit the superscript ‘‘M’’ for equilibrium propagators and self-energies.

² 4×4 Nambu matrices are denoted by a widehat, while 2×2 spin matrices are denoted by a narrow hat.

³ We set $k_B = \hbar = 1$ throughout this report.

⁴ See Ref. [27] for a details on these symmetry relations.

⁵ In the hole-sector $\vec{\sigma}^{\text{tr}} = -\sigma_y \vec{\sigma}_y \sigma_y$ is the transpose of the Pauli matrices

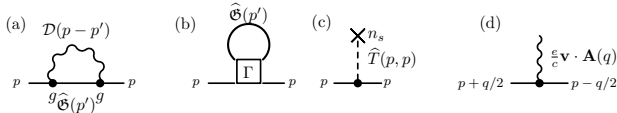


FIG. 1. Leading self-energy diagrams in the quasiclassical theory of superconductivity. (a) electron-phonon self energy, (b) mean-field electron-electron self energy, (c) electron-impurity self energy in the T-matrix approximation, and (d) the coupling of charge currents to an electromagnetic field with $q = (\mathbf{q}, \omega_m)$.

a matrix transport-type equation for the quasiclassical Matsubara propagator defined in Eq. (1) [23],

$$\left[i\varepsilon_n \hat{\tau}_3 - \hat{\Sigma}(\mathbf{p}, \mathbf{r}; \varepsilon_n), \hat{\mathcal{G}}(\mathbf{p}, \mathbf{r}; \varepsilon_n) \right] + i\hbar \mathbf{v}_\mathbf{p} \cdot \nabla \hat{\mathcal{G}}(\mathbf{p}, \mathbf{r}; \varepsilon_n) = 0. \quad (9)$$

In contrast to Gorkov's equation, which is a second-order differential equation with a unit source term originating from the Fermion anti-commutation relations, Eilenberger's equation is a homogeneous, first-order differential equation describing the evolution of the matrix propagator along classical trajectories defined by the Fermi velocity, $\mathbf{v}_\mathbf{p} = \nabla_{\mathbf{p}} \xi_{\mathbf{p}}$. The physical solutions to the transport equation satisfy Eilenberger's normalization condition [23],

$$\hat{\mathcal{G}}(\mathbf{p}, \mathbf{r}; \varepsilon_n)^2 = -\pi^2 \hat{1}, \quad (10)$$

which enforces conservation of the spectral weight within the bandwidth of low-energy excitations.

B. Self Energies

The physical properties of a particular superconducting material are encoded in the self energy, $\hat{\Sigma}(\mathbf{p}, \mathbf{r}; \varepsilon_n)$, that enters Eq. (9). To leading order in the small expansion parameters of quasiclassical theory, $s = \{k_B T/E_f, \hbar/p_f \xi_0, \hbar/\tau E_f, \hbar\omega/E_f, \frac{e}{c} v_f A(\omega)/E_f\}$, the processes that define the self-energy are represented by Feynman diagrams for electron-phonon, electron-electron and electron-impurity interactions or the coupling to external fields, are shown in Fig. 1.

1. Pairing Self-Energy

The electron-phonon self-energy, Fig.1(a), is central to the theory of superconductivity in elemental superconductors such as Al, Nb, Ta. Phonon-mediated electron-electron interactions in the Cooper channel are often sufficiently attractive, and retarded in time, to overcome the repulsive electron-electron interaction in the Cooper channel, Fig.1(b). For these superconductors the dominant pairing channel is the spin-singlet ($S = 0$), orbital A_{1g} channel, i.e. the identity representation. In what follows we consider pairing mediated by a net attractive interaction in the spin-singlet ($S = 0$), isotropic "s-wave" ($L = 0$) channel, $g(\varepsilon_n; \varepsilon'_n)$, which gives rise to a macroscopic pairing amplitude and mean-field pairing self energy

$$\Delta(\mathbf{r}; \varepsilon_n) = T \sum_{n'} g(\varepsilon_n - \varepsilon_{n'}) \int dS_{\mathbf{p}'} f(\mathbf{p}', \mathbf{r}; \varepsilon_{n'}), \quad (11)$$

where $g(\omega_m) \equiv \lambda(\omega_m) - \mu^*$, with $\lambda(\omega_m)$ the phonon-mediated electron-electron interaction, and μ^* the repulsive Coulomb pseudopotential [27]. Note that $\lambda(\omega_m)$ provides a natural cutoff at the maximum phonon energy ω_D .

For Nb, Ta and Al, with $T_c/\omega_D \ll 1$, the effects of retardation are small, and that also holds for the electromagnetic response of Nb at microwave frequencies, $\hbar\omega \ll 2\Delta_0$ [33]⁶. Thus, for our purposes we can approximate $g(\varepsilon_n - \varepsilon_{n'}) = g\Theta(\omega_D - |\varepsilon_n|)\Theta(\omega_D - |\varepsilon_{n'}|)$, in which case we obtain the weak-coupling gap equation for the pairing self energy,

$$\Delta(\mathbf{r}) = g T \sum_{n'}^{|\varepsilon_{n'}| \leq \omega_D} \int dS_{\mathbf{p}'} f(\mathbf{p}', \mathbf{r}; \varepsilon_{n'}), \quad (12)$$

where for any self energy functional, the pair propagator, $f(\mathbf{p}, \mathbf{r}; \varepsilon_n)$, is obtained from the solution of Eilenberger's transport equation (9) and normalization condition (10).

2. Electron-Impurity Self-Energy

The effects of disorder on superconductivity result from electron scattering off a random distribution of impurities. The electron-impurity self-energy is determined by the forward scattering limit of the electron-impurity T-matrix and the mean impurity density, n_s ,

$$\hat{\Sigma}_{\text{imp}}(\mathbf{p}; \varepsilon_n) = n_s \hat{T}(\mathbf{p}, \mathbf{p}; \varepsilon_n), \quad (13)$$

where the T-matrix for electron-impurity scattering satisfies a Bethe-Salpeter (BS) equation, shown diagrammatically in Fig. 2 and given by

$$\begin{aligned} \hat{T}(\mathbf{p}', \mathbf{p}; \varepsilon_n) &= \hat{U}(\mathbf{p}', \mathbf{p}) \\ &+ N_f \int dS_{\mathbf{p}''} \hat{U}(\mathbf{p}', \mathbf{p}'') \hat{\mathcal{G}}(\mathbf{p}'', \varepsilon_n) \hat{T}(\mathbf{p}'', \mathbf{p}; \varepsilon_n). \end{aligned} \quad (14)$$

This equation encodes the effects of multiple scattering by a *single* impurity, with the intermediate states defined by the self-consistently determined Nambu matrix propagator for both quasiparticles and pairs.

In what follows we consider random distributions of uncorrelated impurities with concentrations of non-magnetic and paramagnetic impurities with mean densities c_N and c_S , respectively. For isotropic impurity potentials the non-magnetic electron-impurity vertex is $V(\mathbf{p}, \mathbf{p}')\hat{1}$, while that for spin-exchange scattering is $J(\mathbf{p}, \mathbf{p}')\vec{S} \cdot \vec{s}$. Both matrix elements are parametrized by scattering amplitudes in orbital angular momentum channels, $X(\mathbf{p}, \mathbf{p}') = \sum_{l \geq 0} (2l + 1) X_l P_l(\hat{\mathbf{p}} \cdot \hat{\mathbf{p}}')$, for $X = V, J$, where $\{P_l(x) | l = 0, 1, 2, \dots\}$ are Legendre polynomials. Amplitudes V_l and J_l define normal-state quasiparticle-impurity scattering phase shifts $\delta_{Nl} = \tan^{-1} \bar{v}_{Nl}$ where $\bar{v}_{Nl} = \pi N_f V_l$, $\delta_{Sl}^{\pm} = \pm \tan^{-1} \bar{u}_{Sl}$ where $\bar{u}_{Sl} = \pi N_f J_l S \frac{\hbar}{2}$. and $+$ ($-$) corresponds to the electron spin aligned parallel (anti-parallel) to the impurity spin \vec{S} .

The number of relevant channels is determined by the ratio of the atomic radius of the impurity and the Fermi wavelength, i.e. $l \leq \text{Int}[k_f R]$, where $k_f = p_f/\hbar$ is the Fermi wavevector [35]. Typical values for impurities in metals are $k_f R \approx 1 - 2$ [36] In what follows we retain only one channel, i.e. the s-wave ($l = 0$) channel. We also treat paramagnetic impurities as classical spins. The impurity spins are unordered, in which case we average over the spin orientations of the ensemble of paramagnetic impurities. Thus, $\langle S_i \rangle = 0$, $\langle S_i S_j \rangle = S^2 \frac{1}{3} \delta_{ij}$, etc.

⁶ At much higher frequencies phonons are observable in the optical absorption spectrum for frequencies just above the gap [27, 34].

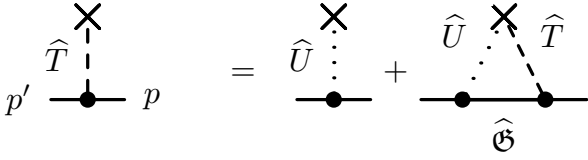


FIG. 2. T-matrix for multiple scattering of quasiparticles and pairs by an impurity with transition matrix $\hat{U}(\mathbf{p}', \mathbf{p})$. Intermediate states are described by the quasiclassical propagator, $\hat{\mathcal{G}}(\mathbf{p}, \epsilon_n)$.

C. Equilibrium Propagator and Self Energies

For spatially homogeneous superconducting states, $\nabla\hat{\mathcal{G}} = 0$, the propagator satisfies two matrix equations,

$$\left[i\epsilon_n \hat{\tau}_3 - \hat{\Delta} - \hat{\Sigma}_{\text{imp}}, \hat{\mathcal{G}} \right] = 0, \quad \text{and} \quad \hat{\mathcal{G}}^2 = -\pi^2 \hat{1}. \quad (15)$$

Thus, for a spatially homogeneous spin-singlet s-wave superconductor in the *clean limit* ($\hat{\Sigma}_{\text{imp}} = 0$) the pairing self energy is given by $\hat{\Delta} = \Delta \hat{\tau}_1 i\sigma_y$, where the $U(1)_N$ gauge freedom allows us fix the phase of Δ to be real, in which case only the $\hat{\tau}_1$ matrix appears. The corresponding solution to Eqs.(15) for the propagator is

$$\hat{\mathcal{G}}(\epsilon_n) = -\pi \frac{i\epsilon_n \hat{\tau}_3 - \hat{\Delta}}{\sqrt{\epsilon_n^2 + \Delta^2}}, \quad (\text{clean limit}) \quad (16)$$

$$\text{where} \quad \Delta = g \frac{\pi}{\beta} \sum_n^{\omega_D} \frac{\Delta}{\sqrt{\epsilon_n^2 + \Delta^2}}, \quad (17)$$

is the mean-field “gap function” in the weak-coupling approximation, g is the pairing interaction in the spin-singlet, s-wave channel and ω_D is the bandwidth of attraction. Standard regularization of the log-divergent sum for $\omega_D/T \rightarrow \infty$ allows us to eliminate the coupling constant, g , and the bandwidth ω_D in favor of the measurable clean limit transition temperature, T_{c0} . The Matsubara sum now converges on the low-energy scale set by $T_{c0}, \Delta \ll \omega_D$,

$$\ln \left(\frac{T}{T_{c0}} \right) = 2\pi T \sum_{n=0}^{\infty} \left[\frac{1}{\sqrt{\epsilon_n^2 + \Delta^2}} - \frac{1}{|\epsilon_n|} \right]. \quad (18)$$

1. Non-Magnetic Impurities

For non-magnetic impurities configurational averaging is defined by a joint probability distribution for the random positions of the impurities. For concentrations of *uncorrelated* impurities the configurational averaged T-matrix reduces to the following BS equation for scattering restricted to the s-wave channel,

$$\hat{T}_N = v_N \hat{1} + N_f v_N \langle \hat{\mathcal{G}}(\mathbf{p}, \epsilon_n) \rangle \hat{T}_N, \quad (19)$$

where v_N is the matrix element for electron-impurity scattering by non-magnetic impurities in the s-wave channel, and $\langle \hat{\mathcal{G}}(\mathbf{p}, \epsilon_n) \rangle$ is the Fermi surface average of the propagator, $\hat{\mathcal{G}}(\mathbf{p}, \epsilon_n)$. In general the propagator is anisotropic, even for conventional BCS superconductors such as Nb. Non-magnetic impurities are pair-breaking in anisotropic superconductors, including anisotropic BCS superconductors, as described in some detail in Ref. [37]. However, for isotropic

(“s-wave”), spin-singlet superconductivity $\langle \hat{\mathcal{G}} \rangle = \hat{\mathcal{G}}(\epsilon_n)$, in which case the T-matrix in Eq. (19) is easily obtained using the normalization condition in Eq. (10),

$$\hat{T}_N = \frac{1}{\pi N_f} \left\{ \frac{\bar{v}_N}{1 + \bar{v}_N^2} \hat{1} + \frac{\bar{v}_N^2}{1 + \bar{v}_N^2} \hat{\mathcal{G}}(\epsilon_n) \right\}, \quad (20)$$

where $\bar{v}_N \equiv \pi N_f v_N$. This result is often expressed in terms of the s-wave scattering phase shift $\delta_N = \tan^{-1} \bar{v}_N$,

$$\hat{T}_N = \frac{1}{\pi N_f} \left\{ \sin \delta_N \cos \delta_N \hat{1} + \sin^2 \delta_N \hat{\mathcal{G}}(\epsilon_n) \right\}. \quad (21)$$

The unit matrix term in \hat{T}_N does not contribute to the impurity self-energy because it drops out of Eilenberger’s Eq. (15). Thus,

$$\hat{\Sigma}_N = \frac{1}{2\tau_N} \hat{\mathcal{G}}, \quad (22)$$

where the quasiparticle-impurity scattering rate is

$$\frac{1}{2\tau_N} = \frac{c_N}{\pi N_f} \frac{\bar{v}_N^2}{1 + \bar{v}_N^2} \equiv \Gamma_N \sin^2 \delta_N, \quad (23)$$

which in the unitarity limit becomes,

$$\frac{1}{2\tau_N} \xrightarrow{|\bar{v}_N| \rightarrow \infty} \Gamma_N \equiv \frac{c_N}{\pi N_f}. \quad (24)$$

2. Paramagnetic Impurities

For paramagnetic impurities the self-energy is defined by an additional configurational average of the T-matrix over the probability distribution of impurity spin directions,

$$\hat{\Sigma}_S(\epsilon_n) = c_S \int \frac{d\Omega_{\vec{S}}}{4\pi} \hat{T}(\epsilon_n; \vec{S}) \equiv c_S \hat{T}_S(\epsilon_n), \quad (25)$$

where $\hat{T}(\epsilon_n; \vec{S})$ describes multiple scattering of quasiparticles and Cooper pairs by a single *polarized* magnetic impurity with spin $\vec{S} = S\vec{e}$ where $\vec{e} \cdot \vec{e} = e^i e^i = 1$. The ensemble average over a uniform probability distribution for the directions of the impurity spins defines the T-matrix for the unpolarized distribution of *paramagnetic* impurities, $\hat{T}_S(\epsilon_n)$.

The symmetry constraints of a homogeneous paramagnetic impurity distribution imply that $\hat{T}_S(\epsilon_n)$ contains only terms proportional to $\hat{\tau}_3$ and $\hat{\tau}_1 i\sigma_y$. In particular, (i) there are no terms proportional to $i\hat{\tau}_2 i\sigma_y$, as such a term would break time-reversal symmetry by the renormalized gap amplitude, and (ii) there are no spin-triplet terms proportional to $\hat{\tau}_1 i\vec{\sigma}$, which would break spin-rotation symmetry. Thus, the paramagnetic impurity self-energy includes only these terms,

$$\hat{\Sigma}_S(\epsilon_n) = \Sigma_S(\epsilon_n) \hat{\tau}_3 + \Delta_S(\epsilon_n) \hat{\tau}_1 i\sigma_y. \quad (26)$$

The quasiclassical propagator then has the same Nambu matrix structure as the clean-limit propagator in the Eq. (16),

$$\hat{\mathcal{G}}(\epsilon_n) = -\pi \frac{i\tilde{\epsilon}_n \hat{\tau}_3 - \tilde{\Delta} \hat{\tau}_1 i\sigma_y}{\sqrt{\tilde{\epsilon}_n^2 + \tilde{\Delta}^2}}, \quad (27)$$

where the renormalized Matsubara frequency and pairing self energy are given by

$$i\tilde{\epsilon}_n = i\epsilon_n - \Sigma_N(\epsilon_n) - \Sigma_S(\epsilon_n), \quad (28)$$

$$\tilde{\Delta} = \Delta + \Delta_N(\epsilon_n) + \Delta_S(\epsilon_n). \quad (29)$$

To compute the impurity self energy in Eq. (25) we need to construct a BS equation for the configurational averaged T-matrix, $\hat{T}_S(\epsilon_n)$.

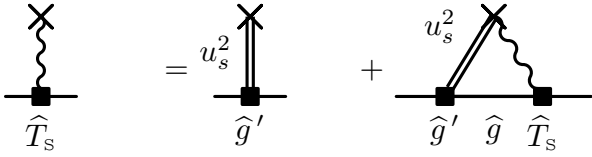


FIG. 3. Configurational averaged T-matrix for scattering of quasiparticles and pairs from an impurity selected from an ensemble of paramagnetic impurities. The leading order term is defined by the vertex $u_s^2 \hat{g}'$ and intermediate states are described by the configurational averaged quasiclassical propagator, $\hat{g} = N_f \hat{\mathcal{G}}$.

3. Bethe-Salpeter Equation for $\hat{T}_S \equiv \langle \hat{T}(\epsilon_n; \vec{S}) \rangle$

We start from the BS equation for $\hat{T}(\epsilon_n; \vec{S})$ in Eq. (14) for multiple scattering of quasiparticles and Cooper pairs by a magnetic impurity with spin \vec{S} . We expand \hat{T} as an infinite series in the spin-exchange interaction matrix element,

$$\hat{T} = \hat{U} + \hat{U} \hat{g} \hat{U} + \hat{U} \hat{g} \hat{U} \hat{g} \hat{U} + \dots, \quad (30)$$

where

$$\hat{U} = u_s \vec{e} \cdot \hat{\Sigma}, \quad \hat{\Sigma} = \begin{pmatrix} \vec{\sigma} & 0 \\ 0 & \vec{\sigma}^{\text{tr}} \end{pmatrix}, \quad (31)$$

with $u_s \equiv J \frac{\hbar}{2} S$ and $\hat{g} \equiv N_f \hat{\mathcal{G}}$. The equilibrium propagator can be expressed in terms of the quasiparticle and pair propagators,

$$\hat{g} = N_f \hat{\mathcal{G}} = g_3 \hat{\tau}_3 + g_1 \hat{\tau}_1 i \sigma_y, \quad (32)$$

$$g_3 = -\pi N_f \frac{i \tilde{\epsilon}_n}{\sqrt{\tilde{\epsilon}_n^2 + \tilde{\Delta}^2}}, \quad (33)$$

$$g_1 = +\pi N_f \frac{\tilde{\Delta}}{\sqrt{\tilde{\epsilon}_n^2 + \tilde{\Delta}^2}}, \quad (34)$$

which satisfy the normalization condition,

$$\hat{g}^2 = (g_3^2 - g_1^2) \hat{1} = -\pi^2 N_f^2 \hat{1}. \quad (35)$$

We carry out the configurational average over the ensemble of paramagnetic impurities term by term in Eq. (30). The first-order term vanishes by symmetry,

$$\langle \hat{U} \rangle = \int \frac{d\Omega_{\vec{e}}}{4\pi} u_s \vec{e} \cdot \hat{\Sigma} \equiv 0. \quad (36)$$

This extends to all terms odd in $\hat{U} \sim \vec{e} \cdot \hat{\Sigma}$. Thus, the leading order term for the configurational averaged T-matrix is 2nd order in u_s ,

$$\langle \hat{U} \hat{g} \hat{U} \rangle = u_s^2 \int \frac{d\Omega_{\vec{e}}}{4\pi} e^i e^j \hat{\Sigma}^i \hat{g} \hat{\Sigma}^j = u_s^2 \frac{1}{3} \hat{\Sigma}^i \hat{g} \hat{\Sigma}^i \equiv u_s^2 \hat{g}'. \quad (37)$$

It is straightforward to show that

$$\hat{g}' = N_f \hat{\mathcal{G}}' = g_3 \hat{\tau}_3 - g_1 \hat{\tau}_1 i \sigma_y. \quad (38)$$

Comparing this result with Eq. (32) we see that the 2nd order Born scattering term leads to a sign change in the off-diagonal spin-singlet pairing self energy, and is responsible for pair breaking from this double spin-exchange process. Note that \hat{g}' also satisfies the normalization condition, $(\hat{g}')^2 = -\pi^2 N_f^2 \hat{1}$.

Similarly, the 4th order contribution to the configurational averaged T-matrix reduces to,

$$\langle \hat{U} \hat{g} \hat{U} \hat{g} \hat{U} \hat{g} \hat{U} \rangle = u_s^2 \hat{g}' \times \hat{g} \times u_s^2 \hat{g}', \quad (39)$$

and similarly for all even powers of \hat{U} . The resulting configurational averaged T-matrix satisfies the BS equation,

$$\hat{T}_S = u_s^2 \hat{g}' + u_s^2 \hat{g}' \times \hat{g} \times \hat{T}_S, \quad (40)$$

shown diagrammatically in Fig. 3. The formal solution for \hat{T}_S is then,

$$\hat{T}_S = \left(\hat{1} - u_s^2 \hat{g}' \hat{g} \right)^{-1} \times u_s^2 \hat{g}'. \quad (41)$$

The matrix inverse $\left(\hat{1} - u_s^2 \hat{g}' \hat{g} \right)^{-1}$ is easily obtained by making use of the normalization conditions, $(\hat{g})^2 = (\hat{g}')^2 = -\pi^2 N_f^2 \hat{1}$, and the anti-commutator,

$$\{\hat{g}, \hat{g}'\} = 2(g_3^2 - g_1^2) \hat{1} = 2\pi^2 N_f^2 \left\{ 1 - 2 \frac{\tilde{\epsilon}_n^2}{\tilde{\epsilon}_n^2 + \tilde{\Delta}^2} \right\} \hat{1}, \quad (42)$$

where the second equality follows from Eqs. (33)-(34). Thus, it is straight-forward to construct the inverse,

$$\left(\hat{1} - u_s^2 \hat{g}' \hat{g} \right)^{-1} = \frac{\left(\hat{1} - u_s^2 \hat{g} \hat{g}' \right)}{(1 - \bar{u}_s^2)^2 + 4\bar{u}_s^2 \left(\frac{\tilde{\epsilon}_n^2}{\tilde{\epsilon}_n^2 + \tilde{\Delta}^2} \right)}, \quad (43)$$

where $\bar{u}_s \equiv \pi N_f u_s$. We then obtain the configurational averaged T-matrix,

$$\begin{aligned} \hat{T}_S &= u_s^2 \frac{\bar{u}_s^2}{(1 - \bar{u}_s^2)^2 + 4\bar{u}_s^2 \left(\frac{\tilde{\epsilon}_n^2}{\tilde{\epsilon}_n^2 + \tilde{\Delta}^2} \right)} \times \hat{g} \\ &+ u_s^2 \frac{1}{(1 - \bar{u}_s^2)^2 + 4\bar{u}_s^2 \left(\frac{\tilde{\epsilon}_n^2}{\tilde{\epsilon}_n^2 + \tilde{\Delta}^2} \right)} \times \hat{g}'. \end{aligned} \quad (44)$$

This result when multiplied by the paramagnetic impurity density, n_s , and analytically continued to the real energies: $i\epsilon_n \rightarrow \epsilon + i0^+$, is equivalent to Shiba's Eq. (3.6) [20] for the self energy. The poles and branch cuts of $\hat{T}_S^R(\epsilon) = \hat{T}_S(\epsilon_n \rightarrow -i\epsilon + 0^+)$ reveal the spectrum of both continuum excitations and sub-gap bound states. In particular, in the limit, $c_s \rightarrow 0$ (isolated impurities), we can neglect the impurity renormalization of ϵ and Δ , in which case the denominator of $\hat{T}_S^R(\epsilon)$ has branch cuts at continuum edges, $\pm\Delta$, and isolated poles at sub-gap energies,

$$\epsilon^\pm = \pm\Delta \frac{1 - \bar{u}_s^2}{1 + \bar{u}_s^2}, \quad (45)$$

corresponding to quasiparticle states bound to the impurity with wave functions of radial extent of order $\xi_S = \xi_0 / |\sin(\delta^+ - \delta^-)|$, where $\xi_0 = \hbar v_f / \pi \Delta_0$ is the zero-temperature coherence length in the clean limit, and the phase shifts for pure exchange scattering are defined by $\tan \delta^\pm = \pm \bar{u}_s$. Thus, for $\bar{u}_s = \pm 1$ there is a bound state at the Fermi energy with radial extent ξ_0 . For $0 < |\bar{u}_s| < 1$ the bound state energy lies in the gap and the wave function spreads radially. This result is equivalent to that of Rusinov [21] for impurities with pure exchange interactions with quasiparticles.

For a finite concentration of paramagnetic impurities the bound states hybridize, generating an inhomogeneous band of quasiparticle states centered near the single-impurity bound state energy. The bandwidth and spectral weight of these sub-gap states is encoded in the renormalization of ε and Δ by the impurity self energy,

$$\widehat{\Sigma}_S \equiv c_S \widehat{T}_S(\varepsilon_n) = \Sigma_S \widehat{\tau}_3 + \Delta_S \widehat{\tau}_1 i\sigma_y. \quad (46)$$

Note that the first term in Eq. (44), proportional to \widehat{g} , is a correction to the potential scattering T-matrix from the exchange interaction. For isotropic, spin-singlet superconductors this term is non-pair-breaking and drops out of the equilibrium Eilenberger equation (9), and thus does not contribute to pair breaking and the sub-gap spectrum. However, this exchange correction, as well as the non-magnetic impurity scattering self energy, does contribute to the non-equilibrium response functions, and thus to the microwave conductivity as we discuss in Sec. III. Thus, we retain both sets of terms in the self energy obtained from the configurational averaged T-matrix,

$$\Sigma_{\text{imp}} \equiv \Sigma_N + \Sigma_S = -\frac{1}{2\tau_1} \frac{i\tilde{\varepsilon}_n}{\sqrt{\tilde{\varepsilon}_n^2 + \tilde{\Delta}^2}}, \quad (47)$$

$$\Delta_{\text{imp}} \equiv \Delta_N + \Delta_S = +\frac{1}{2\tau_2} \frac{\tilde{\Delta}}{\sqrt{\tilde{\varepsilon}_n^2 + \tilde{\Delta}^2}}, \quad (48)$$

where the scattering rates are given by

$$\frac{1}{\tau_1} = \frac{1}{\tau_N} + \frac{1}{\tau_S} \frac{1 + \tilde{u}_S^2}{(1 + \tilde{u}_S^2)^2 - 4\tilde{u}_S^2 \left(\frac{\tilde{\Delta}^2}{\tilde{\varepsilon}_n^2 + \tilde{\Delta}^2} \right)}, \quad (49)$$

$$\frac{1}{\tau_2} = \frac{1}{\tau_N} - \frac{1}{\tau_S} \frac{1 - \tilde{u}_S^2}{(1 + \tilde{u}_S^2)^2 - 4\tilde{u}_S^2 \left(\frac{\tilde{\Delta}^2}{\tilde{\varepsilon}_n^2 + \tilde{\Delta}^2} \right)}, \quad (50)$$

$$\text{with } \frac{1}{2\tau_N} = \frac{c_N}{\pi N_f} \frac{\tilde{v}_N^2}{1 + \tilde{v}_N^2} \text{ and } \frac{1}{2\tau_S} = \frac{c_S}{\pi N_f} \tilde{u}_S^2, \quad (51)$$

are the normal-state scattering rate for non-magnetic impurities with density c_N , and the Born scattering rate for paramagnetic impurities with density c_S . Equations (49) and (50) are not restricted to the Born approximation. The dimensionless matrix elements, $\tilde{v}_N = \pi N_f v_N$ and $\tilde{u}_S = \pi N_f u_S$ are measures of the strength of the potential and exchange interaction between quasiparticles and impurities. Equations (47), (48), when analytically continued to the real energy axis, $i\varepsilon_n \rightarrow \varepsilon + i0^+$, agree with Shiba's Eqs. (3.6) and (3.7) for pure exchange scattering by a distribution of paramagnetic impurities. And if we retain only terms of order \tilde{u}_S^2 in Eqs. (47) and (48) we obtain the Born limit studied by Abrikosov and Gorkov (AG). Thus, the renormalized Matsubara energy and pairing self energy become,

$$\tilde{\varepsilon}_n = \varepsilon_n + \frac{1}{2\tau_1} \frac{\tilde{\varepsilon}_n}{\sqrt{\tilde{\varepsilon}_n^2 + \tilde{\Delta}^2}}, \quad (52)$$

$$\tilde{\Delta} = \Delta + \frac{1}{2\tau_2} \frac{\tilde{\Delta}}{\sqrt{\tilde{\varepsilon}_n^2 + \tilde{\Delta}^2}}. \quad (53)$$

We introduce renormalization factors: $\tilde{\varepsilon}_n \equiv Z_3(\varepsilon_n) \varepsilon_n$ and $\tilde{\Delta} \equiv Z_1(\varepsilon_n) \Delta$, and obtain coupled transcendental equations for $Z_{1,3}$ to be solved as functions of ε_n , Δ , $1/\tau_N$ and $1/\tau_S$.

The difference in scattering rates in Eqs. (52) and (53) implies $Z_3 \neq Z_1$, and the violation of Anderson's theorem, the suppression of T_c , pair-breaking and the existence of quasiparticle states in the gap.

Note that the renormalized scattering rates, $1/\tau_{1,2}$, depend only on the ratio $Z = Z_3/Z_1$, in which case Eqs. (49) and (50) become,

$$\frac{1}{\tau_1} = \frac{1}{\tau_N} + \frac{1}{\tau_S} \frac{1 + \tilde{u}_S^2}{(1 + \tilde{u}_S^2)^2 - 4\tilde{u}_S^2 \left(\frac{\Delta^2}{\tilde{\varepsilon}_n^2 + \Delta^2} \right)}, \quad (54)$$

$$\frac{1}{\tau_2} = \frac{1}{\tau_N} - \frac{1}{\tau_S} \frac{1 - \tilde{u}_S^2}{(1 + \tilde{u}_S^2)^2 - 4\tilde{u}_S^2 \left(\frac{\Delta^2}{\tilde{\varepsilon}_n^2 + \Delta^2} \right)}, \quad (55)$$

$$\text{where } \frac{\tilde{\varepsilon}_n}{\tilde{\Delta}} = \frac{Z_3}{Z_1} \frac{\varepsilon_n}{\Delta} \equiv \frac{\bar{\varepsilon}_n}{\bar{\Delta}}. \quad (56)$$

We obtain $\bar{\varepsilon}_n$ from the ratio of Eq. (52) and Eq. (53),

$$\bar{\varepsilon}_n = \varepsilon_n + \frac{1}{2} \left(\frac{1}{\tau_1} - \frac{1}{\tau_2} \right) \frac{\bar{\varepsilon}_n}{\sqrt{\bar{\varepsilon}_n^2 + \bar{\Delta}^2}} \equiv \varepsilon_n + \frac{1}{\tau_S} \frac{\bar{\varepsilon}_n}{\sqrt{\bar{\varepsilon}_n^2 + \bar{\Delta}^2}}, \quad (57)$$

$$\text{where } \frac{1}{\tau_S} \equiv \frac{1}{\tau_S} \frac{1}{(1 + \tilde{u}_S^2)^2 - 4\tilde{u}_S^2 \left(\frac{\Delta^2}{\tilde{\varepsilon}_n^2 + \Delta^2} \right)}. \quad (58)$$

There are several observations to be made. (i) A key result is that if $1/\tau_1 = 1/\tau_2$ impurity scattering drops out of all equilibrium properties. This is Anderson's theorem. (ii) The flip side is that *only* the difference between the scattering rates $1/\tau_1$ and $1/\tau_2$, which is proportional to the exchange scattering rate $1/\tau_S$, contributes to pair breaking, suppression of T_c and the generation of a spectrum of sub-gap quasiparticles. (iii) Eq. (57) reduces two self-consistency equations for $\tilde{\varepsilon}_n$ and $\tilde{\Delta}$ to one self-consistency equation for $\bar{\varepsilon}$. Note also that Eqs. (57) and (51) reduce to

$$\bar{\varepsilon}_n = \varepsilon_n + \frac{1}{\tau_S} \frac{\bar{\varepsilon}_n \sqrt{\bar{\varepsilon}_n^2 + \bar{\Delta}^2}}{(1 + \tilde{u}_S^2)^2 \bar{\varepsilon}_n^2 + (1 - \tilde{u}_S^2)^2 \bar{\Delta}^2}. \quad (59)$$

Analytic continuation to the real axis, $i\varepsilon_n \rightarrow \varepsilon + i0^+$, highlights the presence of the band of sub-gap states, which in the limit $c_S \rightarrow 0^+$ correspond to the isolated impurity bound states above and below the Fermi level, Eq. (45), found by Rusinov.

4. Suppression of T_c and the Order Parameter Δ

The equilibrium solution to the homogeneous Eilenberger equations including scattering by non-magnetic and paramagnetic impurities reduces to

$$\widehat{\mathcal{G}}(\varepsilon_n) = -\pi \frac{i\tilde{\varepsilon}_n \widehat{\tau}_3 - \Delta \widehat{\tau}_1 i\sigma_y}{\sqrt{\tilde{\varepsilon}_n^2 + \Delta^2}}, \quad (60)$$

$$\text{where } \Delta = \lambda \frac{\pi}{\beta} \sum_n^{\omega_D} \frac{\Delta}{\sqrt{\tilde{\varepsilon}_n^2 + \Delta^2}}, \quad (61)$$

The gap equation now includes the pair-breaking impurity self energy with $\bar{\varepsilon}_n$ defined by Eq. (59). As was done for the gap equation in the clean limit we eliminate the coupling constant and bandwidth in place of T_{c0} ,

$$\ln \left(\frac{T}{T_{c0}} \right) = 2\pi T \sum_{n=0}^{\infty} \left[\frac{1}{\sqrt{\bar{\varepsilon}_n^2 + \bar{\Delta}^2}} - \frac{1}{|\varepsilon_n|} \right]. \quad (62)$$

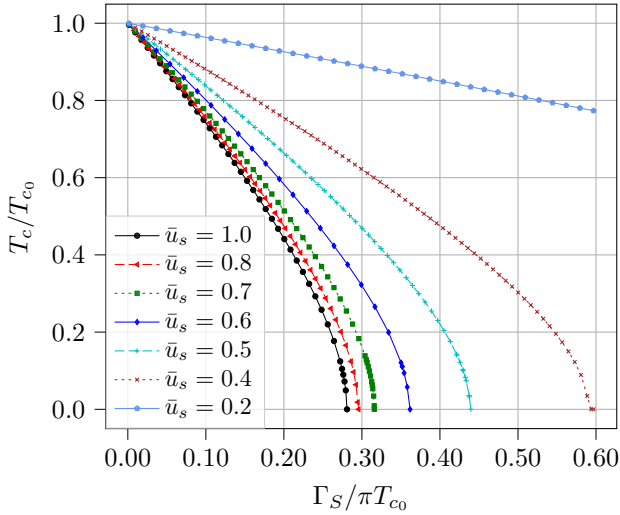


FIG. 4. Suppression of the transition temperature, T_c , as a function of Γ_S (impurity concentration) for a range of \bar{u}_S spanning the Born limit, $\bar{u}_S \ll 1$, to maximal pair-breaking for $\bar{u}_S = 1$.

This equation for Δ and Eq. (59) for $\bar{\epsilon}_n$ must be solved together self-consistently as a function of T/T_{c_0} , the scattering rate $1/\tau_S$, and the exchange interaction \bar{u}_S . The gap parameter $\Delta \rightarrow 0^+$ as $T \rightarrow T_c$ from below. In this limit $\epsilon_n = 2\pi T_c(n + \frac{1}{2})$ and

$$\bar{\epsilon}_n = \text{sgn}(\epsilon_n) \left(|\epsilon_n| + \frac{1}{\bar{\tau}_{S_n}} \right), \quad (63)$$

$$\text{where } \frac{1}{\bar{\tau}_{S_n}} = \frac{1}{\tau_S} \frac{1}{(1 + \bar{u}_S^2)^2} = \Gamma_S \frac{4\bar{u}_S^2}{(1 + \bar{u}_S^2)^2}, \quad (64)$$

is the normal-state quasiparticle-impurity exchange scattering rate, where

$$\Gamma_S \equiv \frac{c_S}{2\pi N_f}, \quad (65)$$

depends on the concentration of paramagnetic impurities and normal-state quasiparticle density of states at the Fermi level, and plays the same role as the unitarity limit for s-wave, non-magnetic impurity scattering in unconventional superconductors [38]. In particular, the paramagnetic scattering rate is maximized with respect to the exchange interaction at $\bar{u}_S^2 = 1$, and thus Γ_S is the maximum scattering rate for fixed concentration. Note also that the scattering rate for $\bar{u}_S^2 > 1$ is equivalent in terms of equilibrium pair-breaking to the scattering rate for an exchange interaction $1/\bar{u}_S^2 < 1$.

The physical significance of $\bar{u}_S^2 = 1$ was pointed out not long after the works of YRS. For a single paramagnetic impurity in a spin-singlet, s-wave superconductor $\bar{u}_S = 1$ corresponds to level crossing at the Fermi level, and was interpreted as a quantum phase transition of the ground state by Sakurai [39]. Salkola et al. [40] carried out a self-consistent analysis for a single impurity spin, including gap suppression near the impurity, and found that the critical point is suppressed, $\bar{u}_S^{\text{critical}} \lesssim 1$. Our self-consistent analysis for dilute concentrations of paramagnetic impurities also shows suppression of the critical point. In this case the transition occurs when the low-energy edge of the positive energy impurity band crosses the Fermi level.

The resulting equation for T_c reduces to

$$\ln(T_{c_0}/T_c) = \psi\left(\frac{1}{2} + \frac{1}{2\pi\bar{\tau}_{S_n}T_c}\right) - \psi\left(\frac{1}{2}\right), \quad (66)$$

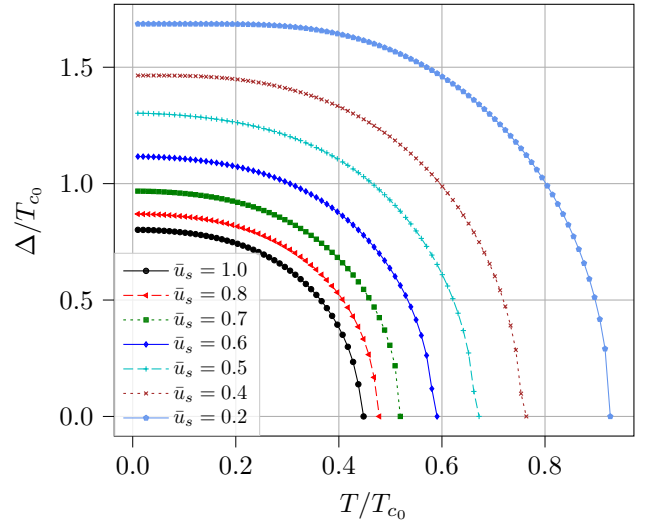


FIG. 5. Pair-breaking suppression of the superconducting gap Δ by paramagnetic impurities for $\Gamma_S/\pi T_{c_0} = 0.2$ and the same range of \bar{u}_S as in Fig. 4.

where $\psi(z)$ is the diGamma function [41]. Equation (66) agrees with the AG result [11] in the Born limit, $\bar{\tau}_{S_n} \rightarrow \tau_S$. The result for the suppression of T_c depends only on the ratio of the exchange scattering rate, $1/\bar{\tau}_{S_n}$, to the pair formation rate, $1/\tau_0 = 2\pi T_{c_0}$. For small scattering rates, $1/2\pi\bar{\tau}_{S_n}T_{c_0} \ll 1$, the suppression of T_c is a small and reduces to,

$$\frac{T_c}{T_{c_0}} \simeq 1 - \frac{\pi^2}{4} \frac{1}{\pi\bar{\tau}_{S_n}T_{c_0}} = 1 - \frac{\pi^2}{4} \frac{\Gamma_S}{\pi T_{c_0}} \frac{4\bar{u}_S^2}{(1 + \bar{u}_S^2)^2}. \quad (67)$$

For sufficiently large exchange scattering rates superconductivity is destroyed at a critical value of the scattering rate $1/\pi\bar{\tau}_{S_n}T_{c_0}|_{\text{crit}} = \frac{1}{2}e^{-\eta} \approx 0.281$. Although T_c/T_{c_0} is a function of $1/\pi\bar{\tau}_{S_n}T_{c_0}$, properties of the superconducting state, including T_c , the gap amplitude, density of states, conductivity etc. generally depend on both the concentration of impurities, c_S , and the exchange interaction, \bar{u}_S .

The suppression of T_c by quasiparticle scattering from paramagnetic impurities is shown in Fig. 4 as a function of $\Gamma_S \propto c_S$ and exchange interaction, \bar{u}_S , the latter ranging from the Born limit to maximal pair-breaking. For fixed impurity concentration the maximum suppression of T_c occurs for $\bar{u}_S^2 = 1$. Similarly, the mean-field order parameter (gap amplitude Δ) defined by the self-consistent solution of Eqs. (62) and (59) is also suppressed relative to the clean limit gap amplitude at all temperatures as show in Fig. 5.

Figure 6 shows the suppression of the transition temperature of niobium for low concentrations of paramagnetic impurities. The small suppression of T_c , even for $\bar{u}_S^2 = 1$, is two orders of magnitude smaller than the suppression of T_c by non-magnetic impurity scattering and gap anisotropy in high-Q superconducting Nb cavities as shown in Fig. 12 of Ref. [37]. However, as we discuss in Sec. III C, in contrast to non-magnetic impurity scattering, very low concentrations of paramagnetic impurities with intermediate exchange coupling can have a major impact on the quality factor and performance of superconducting Nb resonators and devices operating at GHz frequencies and low temperatures.

5. Quasiparticle density of states

The suppression of T_c and Δ is a reflection of the breaking of Cooper pairs by the exchange interaction between the quasi-

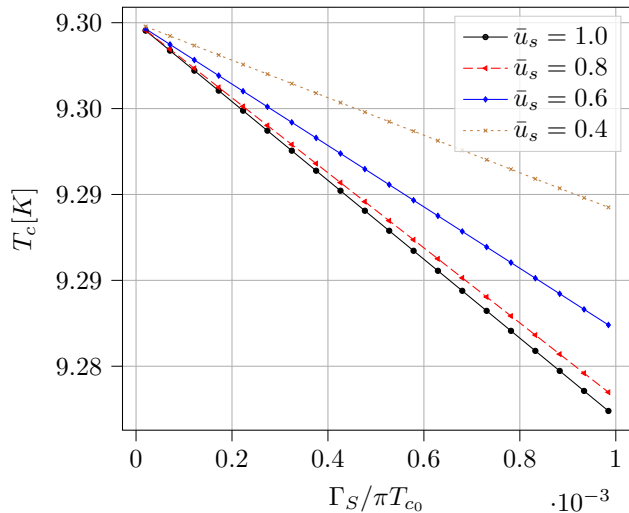


FIG. 6. Weak suppression of T_c for niobium ($T_{c0} = 9.3$ K) for low concentrations of paramagnetic impurities, $\Gamma_S/\pi T_{c0} \leq 10^{-3}$, and \bar{u}_S as shown in the legend.

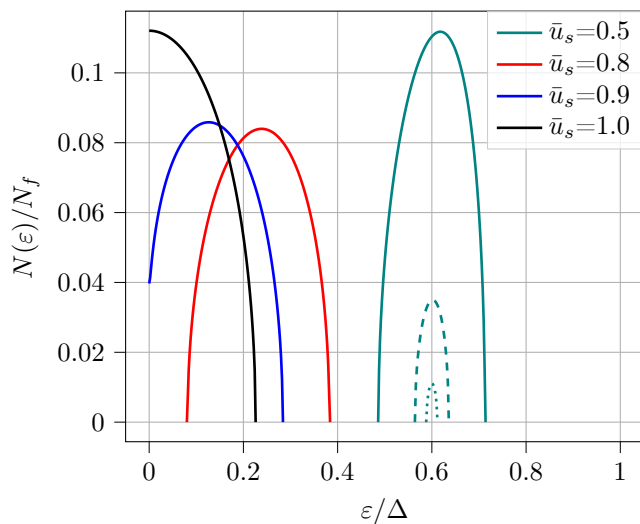


FIG. 7. Density of states for $T/T_c = 0.02$ and $\Gamma_S/2\pi T_{c0} = 3.5 \times 10^{-3}$ (solid lines) shows the shift of the sub-gap band toward the Fermi energy for \bar{u}_S increasing from 0.5 \rightarrow 1.0. The dashed (dotted) line corresponding to $\Gamma_S/2\pi T_{c0} = 3.5 \times 10^{-4}$ (3.5×10^{-5}) shows the reduction in bandwidth and spectral weight for $\bar{u}_S = 0.5$.

particle spin and that of the paramagnetic impurities, and results in the generation of un-paired quasiparticle states with sub-gap energies, $-\Delta < \epsilon < +\Delta$.

The quasiparticle density of states is obtained from the retarded propagator by analytic continuation of the Matsubara propagator in Eq. (60) to the real axis,

$$N(\epsilon) = N_f \text{Im} \frac{\bar{\epsilon}^R(\epsilon)}{\sqrt{\Delta^2 - \bar{\epsilon}^R(\epsilon)^2}}, \quad (68)$$

$$\bar{\epsilon}^R(\epsilon) = \epsilon + 4\Gamma_S \bar{u}_S^2 \frac{\bar{\epsilon}^R(\epsilon) \sqrt{\Delta^2 - \bar{\epsilon}^R(\epsilon)^2}}{(1 - \bar{u}_S^2)\Delta^2 - (1 + \bar{u}_S^2)\bar{\epsilon}^R(\epsilon)^2} \quad (69)$$

The exchange interaction, \bar{u}_S , generates a pair of impurity bands - one above and one below the Fermi level - centered about the energy of an isolated impurity level (Eq. (45)) with bandwidth determined by the impurity density via $\Gamma_S = c_S/2\pi N_f$.

In the Born limit, $\bar{u}_S^2 \ll 1$, the sub-gap spectrum builds from

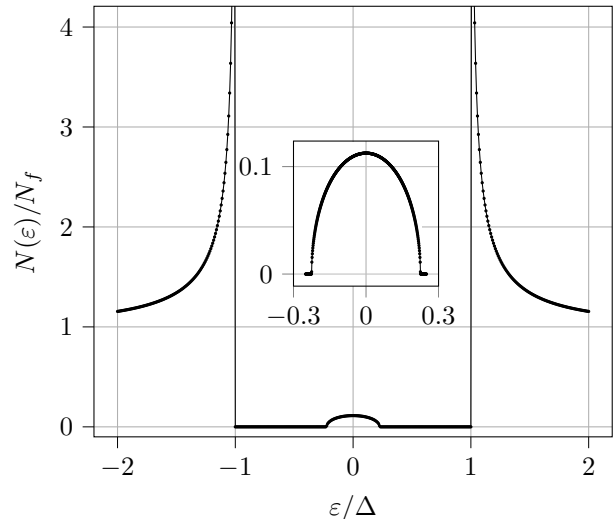


FIG. 8. Quasiparticle density of states for $T/T_c = 0.02$ and exchange coupling, $\bar{u}_S^2 = 1$. The half-width of the sub-gap impurity band, γ , corresponds to $\Gamma_S/2\pi T_{c0} = 3.51 \times 10^{-3}$.

continuum edges at $\pm\Delta$ [42]. With increasing $|\bar{u}_S|$ the impurity band separates from the continuum and shifts toward the Fermi level as shown in Fig. 7. In the limit $\bar{u}_S^2 = 1$, i.e. maximum pair-breaking at fixed c_S , the two bands merge to a single band centered at the Fermi energy defined by the solution of

$$\bar{\epsilon}^R(\epsilon) = \epsilon - \Gamma_S \frac{\sqrt{\Delta^2 - \bar{\epsilon}^R(\epsilon)^2}}{\bar{\epsilon}^R(\epsilon)}. \quad (70)$$

The result is a spectrum of gapless quasiparticle states centered at $\epsilon = 0$ as shown in Fig. (8). The finite DOS at the Fermi level leads to electronic contributions to the heat capacity [43] and thermal conductivity [44] that are linear in T at low temperatures, $T \ll \gamma$, where γ is the half width of the impurity band. The latter is defined by the imaginary part of $\bar{\epsilon}^R(\epsilon) = \epsilon + i\gamma$, which for the band centered at $\epsilon = 0$ is

$$\gamma \simeq \sqrt{\Gamma_S \Delta} \ll \Delta, \quad \text{for } \Gamma_S \ll \Delta. \quad (71)$$

The number of sub-gap states is obtained by integration over the sub-gap energy band,

$$N_{\text{bs}}(\epsilon) = N(0) \sqrt{1 - (\epsilon/\epsilon_{\text{bs}})^2} \Theta(\epsilon_{\text{bs}} - |\epsilon|), \quad (72)$$

with $N(0) = N_f(\epsilon_{\text{bs}}/\Delta)$ and $\epsilon_{\text{bs}} = 2\gamma$, in which case

$$\int_0^{\epsilon_{\text{bs}}} d\epsilon N_{\text{bs}}(\epsilon) = c_S, \quad (73)$$

yielding a pair of quasiparticle states per impurity.

For relatively low impurity concentrations a narrow sub-gap band of states shifts away from the Fermi level as the exchange interaction is reduced. The shift in the position of the impurity band is shown in Fig. (7) for ($\bar{u}_S = 0.5$) to ($\bar{u}_S = 1$) exchange interactions and fixed concentration, $\Gamma_S/2\pi T_{c0} = 3.5 \times 10^{-3}$. Even for intermediate exchange interactions, $\bar{u}_S^2 \approx 1$, low concentrations of paramagnetic impurities do not significantly suppress T_c and the gap amplitude, Δ . However, the low-energy sub-gap states can have a dramatic effects on the conductivity at low temperatures and GHz frequencies, and thus the performance of superconducting devices as discussed in Secs. III C and III D.

III. ELECTROMAGNETIC RESPONSE

The quasiclassical transport equations can be extended to calculate the response functions of a superconductor subject to an electromagnetic field (EM). Here we restrict the analysis to transverse EM fields. The interaction potential is then given by the coupling of the vector potential to the charge current,

$$\widehat{\Sigma}_{\text{EM}}(\mathbf{r}, t) = -\frac{e}{c} \mathbf{v}_{\mathbf{p}} \cdot \mathbf{A}(\mathbf{r}, t) \widehat{\tau}_3, \quad (74)$$

where $e\mathbf{v}_{\mathbf{p}}\widehat{\tau}_3$ is the Nambu charge current operator⁷ and $\mathbf{A}(\mathbf{r}, t)$ satisfies transverse condition, $\nabla \cdot \mathbf{A} = 0$.

The quasiclassical propagator is extended to a function of two frequencies, $\widehat{\mathfrak{G}}(\mathbf{p}, \mathbf{r}; \varepsilon_n) \rightarrow \widehat{\mathfrak{G}}(\mathbf{p}, \mathbf{q}; \varepsilon_n, \omega_m)$, where ω_m is the Bosonic Matsubara frequency associated with Fourier mode \mathbf{q} of the external EM field, $\mathbf{A}(\mathbf{q}, \omega_m)$. Analytic continuation of $\widehat{\mathfrak{G}}(\varepsilon_n; \omega_m)$ to real energies: $i\varepsilon_n \rightarrow \varepsilon + i0^+$ with $i\omega_m \rightarrow \omega + i0^+$ yields the Keldysh propagator [45, 46],

$$\frac{1}{\beta} \sum_{\varepsilon_n} \widehat{\mathfrak{G}}(\varepsilon_n, \omega_m) \xrightarrow{i\omega_m \rightarrow \omega + i0^+} \int_{-\infty}^{+\infty} \frac{d\varepsilon}{4\pi i} \widehat{\mathfrak{G}}^K(\varepsilon; \omega). \quad (75)$$

$$\begin{aligned} \mathbf{J}^R(\mathbf{q}, \omega) = & 2N_f \left(\frac{e^2}{c} \right) \int dS_{\mathbf{p}} \mathbf{v}_{\mathbf{p}} (\mathbf{v}_{\mathbf{p}} \cdot \mathbf{A}(\mathbf{q}, \omega)) \int \frac{d\varepsilon}{4\pi i} \times \\ & \left\{ \frac{\pi^2 d_+^R(\varepsilon, \omega)}{\pi^2 d_+^R(\varepsilon, \omega)^2 + (\mathbf{q} \cdot \mathbf{v}_{\mathbf{p}})^2} \times \left(1 + \frac{\bar{\varepsilon}^R(\varepsilon + \omega) \bar{\varepsilon}^R(\varepsilon) + \Delta^2}{\sqrt{\Delta^2 - \bar{\varepsilon}^R(\varepsilon + \omega)^2} \sqrt{\Delta^2 - \bar{\varepsilon}^R(\varepsilon)^2}} \right) \tanh\left(\frac{\varepsilon}{2T}\right) \right. \\ & - \frac{\pi^2 d_+^A(\varepsilon, \omega)}{\pi^2 d_+^A(\varepsilon, \omega)^2 + (\mathbf{q} \cdot \mathbf{v}_{\mathbf{p}})^2} \times \left(1 + \frac{\bar{\varepsilon}^A(\varepsilon + \omega) \bar{\varepsilon}^A(\varepsilon) + \Delta^2}{\sqrt{\Delta^2 - \bar{\varepsilon}^A(\varepsilon + \omega)^2} \sqrt{\Delta^2 - \bar{\varepsilon}^A(\varepsilon)^2}} \right) \tanh\left(\frac{\varepsilon + \omega}{2T}\right) \\ & \left. + \frac{\pi^2 d_+^a(\varepsilon, \omega)}{\pi^2 d_+^a(\varepsilon, \omega)^2 + (\mathbf{q} \cdot \mathbf{v}_{\mathbf{p}})^2} \times \left(1 + \frac{\bar{\varepsilon}^R(\varepsilon + \omega) \bar{\varepsilon}^A(\varepsilon) + \Delta^2}{\sqrt{\Delta^2 - \bar{\varepsilon}^R(\varepsilon + \omega)^2} \sqrt{\Delta^2 - \bar{\varepsilon}^A(\varepsilon)^2}} \right) \left[\tanh\left(\frac{\varepsilon + \omega}{2T}\right) - \tanh\left(\frac{\varepsilon}{2T}\right) \right] \right\} \quad (77) \end{aligned}$$

where

$$d_+^R = -\frac{1}{\pi} \left[\sqrt{\Delta^2 - \bar{\varepsilon}^R(\varepsilon + \omega)^2} + \sqrt{\Delta^2 - \bar{\varepsilon}^R(\varepsilon)^2} + \frac{1}{\tau_N} - \frac{1}{2} \left(\frac{1}{\tilde{\tau}_S^R(\varepsilon + \omega)} + \frac{1}{\tilde{\tau}_S^R(\varepsilon)} \right) \right], \quad (78)$$

$$d_+^A = -\frac{1}{\pi} \left[\sqrt{\Delta^2 - \bar{\varepsilon}^A(\varepsilon + \omega)^2} + \sqrt{\Delta^2 - \bar{\varepsilon}^A(\varepsilon)^2} + \frac{1}{\tau_N} - \frac{1}{2} \left(\frac{1}{\tilde{\tau}_S^A(\varepsilon + \omega)} + \frac{1}{\tilde{\tau}_S^A(\varepsilon)} \right) \right], \quad (79)$$

$$d_+^a = -\frac{1}{\pi} \left[\sqrt{\Delta^2 - \bar{\varepsilon}^R(\varepsilon + \omega)^2} + \sqrt{\Delta^2 - \bar{\varepsilon}^A(\varepsilon)^2} + \frac{1}{\tau_N} - \frac{1}{2} \left(\frac{1}{\tilde{\tau}_S^R(\varepsilon + \omega)} + \frac{1}{\tilde{\tau}_S^A(\varepsilon)} \right) \right], \quad (80)$$

where $\bar{\varepsilon}^R$ is the analytic continuation of the renormalized Matsubara energy given in Eq. (69), and similarly for $\bar{\varepsilon}^A$; $1/\tau_N$ is the quasiparticle scattering rate by non-magnetic impurities defined in Eq. (51), and

$$\frac{1}{\tilde{\tau}_S^{\text{R,A}}(\varepsilon)} = \frac{1}{\tau_S} (1 - \tilde{u}_S^2) \frac{\Delta^2 - \bar{\varepsilon}^{\text{R,A}}(\varepsilon)^2}{\Delta^2 (1 - \tilde{u}_S^2)^2 - (1 + \tilde{u}_S^2)^2 \bar{\varepsilon}^{\text{R,A}}(\varepsilon)^2} \quad (81)$$

are the retarded and advanced scattering rates contributing to the renormalized gap, $\tilde{\Delta}^{\text{R,A}}$, obtained from analytic continuation of Eq. (50), with $1/\tau_S$ the Born limit scattering rate.

From $\widehat{\mathfrak{G}}^K$ we obtain the retarded (causal) current response as a function of wavevector \mathbf{q} and frequency ω of the EM field,

$$\mathbf{J}^R(\mathbf{q}, \omega) = 2N_f \int dS_{\mathbf{p}} \int \frac{d\varepsilon}{4\pi i} \frac{1}{4} \text{Tr} \{ e\mathbf{v}_{\mathbf{p}} \widehat{\tau}_3 \widehat{\mathfrak{G}}^K(\mathbf{p}, \mathbf{q}; \varepsilon, \omega) \}. \quad (76)$$

The trace is over the charge current operator in Nambu space and the integration is over the Fermi surface and all energies. The Keldysh function encodes both the spectral density of the charge carriers and the occupation of these states, in general for nonequilibrium distributions.

The general theory for the response of superconductors to a transverse EM field in the quasiclassical formalism is developed in Ref. [27], and was applied to superconductors in strong-coupling limit for electron-phonon mediated superconductivity with non-magnetic disorder. The results reported here for the current response of superconductors, with non-magnetic and paramagnetic impurities, is based on the Keldysh propagator calculated in the linear response limit for an isotropic, spin-singlet (“s-wave”) superconductor using Eliashberg’s method [47] of two-frequency analytic continuation [46],

purities.

⁷ The sign convention used here is: $e = -|e|$ is the charge of the electron

$$\sigma(\omega) = \frac{2}{3} N_f \frac{e^2 v_f^2}{i\omega} \int \frac{d\varepsilon}{4\pi i} \left\{ \frac{1}{d_+^R(\varepsilon, \omega)} \times \left(1 + \frac{\bar{\varepsilon}^R(\varepsilon + \omega)\bar{\varepsilon}^R(\varepsilon) + \Delta^2}{\sqrt{\Delta^2 - \bar{\varepsilon}^R(\varepsilon + \omega)^2}\sqrt{\Delta^2 - \bar{\varepsilon}^R(\varepsilon)^2}} \right) \tanh\left(\frac{\varepsilon}{2T}\right) - \frac{1}{d_+^A(\varepsilon, \omega)} \times \left(1 + \frac{\bar{\varepsilon}^A(\varepsilon + \omega)\bar{\varepsilon}^A(\varepsilon) + \Delta^2}{\sqrt{\Delta^2 - \bar{\varepsilon}^A(\varepsilon + \omega)^2}\sqrt{\Delta^2 - \bar{\varepsilon}^A(\varepsilon)^2}} \right) \tanh\left(\frac{\varepsilon + \omega}{2T}\right) + \frac{1}{d_+^A(\varepsilon, \omega)} \times \left(1 + \frac{\bar{\varepsilon}^R(\varepsilon + \omega)\bar{\varepsilon}^A(\varepsilon) + \Delta^2}{\sqrt{\Delta^2 - \bar{\varepsilon}^R(\varepsilon + \omega)^2}\sqrt{\Delta^2 - \bar{\varepsilon}^A(\varepsilon)^2}} \right) \left[\tanh\left(\frac{\varepsilon + \omega}{2T}\right) - \tanh\left(\frac{\varepsilon}{2T}\right) \right] \right\}. \quad (82)$$

B. penetration depth

An EM field incident from the vacuum penetrates a distance of order the London penetration depth, λ , into the superconductor. For type II superconductors in the limit, $\lambda \gg \xi$, the EM field and screening current penetrate well beyond the vacuum-superconducting interface where surface scattering may modify the bulk excitation spectrum in a region of thickness of order the coherence length, ξ , near the interface. The relevant wave vectors contributing to the current response are $0 \leq |\mathbf{q}| \lesssim \pi/\lambda$. Thus, to good approximation we can calculate the current response to the penetrating EM field as the response of the homogeneous, bulk superconductor in the long wavelength, $q \rightarrow 0$, limit. As a result the zero-frequency limit of the imaginary part of the conductivity determines the static London penetration depth, including the effects of disorder, $1/\lambda^2 = (4\pi/c^2) \lim_{\omega \rightarrow 0} \omega \text{Im} \sigma(\omega) \equiv 4\pi n_s(T) e^2/m^* c^2$, where $n_s(T)$ is the superfluid fraction that defines the magnitude of the static supercurrent, and m^* is the normal-state quasiparticle effective mass. The effects of impurity disorder on the superfluid fraction of conventional superconductors have been studied in detail [13]. Although T_c , $\Delta(T)$ and the DOS are unaffected by non-magnetic impurities for isotropic superconductors, the presence of condensate flow relative to the random potential is pair breaking, leading to suppression of the superfluid fraction at all temperatures. Spin-exchange scattering by paramagnetic impurities suppresses T_c , Δ and generates a spectrum of sub-gap quasiparticles even for zero condensate flow. Spin-exchange scattering also contributes to the suppression of the superfluid density as discussed below.

For a microwave EM field the penetration of the field as a function of frequency and temperature is given by

$$\frac{1}{\lambda(\omega, T)^2} = \frac{4\pi}{c^2} \omega \text{Im} \sigma(\omega) \equiv 4\pi \frac{n_s(T, \omega) e^2}{m^* c^2}. \quad (83)$$

In Fig. 9 we show results for $n_s(T, \omega)$ for $\omega = 0.005 T_c$ for low [$\log(\Gamma_N/\pi T_{c0}) = -8.29$] and moderate [$\log(\Gamma_N/\pi T_{c0}) = -0.29$] concentrations of non-magnetic impurities, and for four concentrations of paramagnetic impurities in the limit $\bar{u}_S = 1$, [$\log(\Gamma_S/2\pi T_{c0}) = -4.45, -3.06, -2.45, -2.05$]. The suppression of the superfluid density at $T = 0$ from $n_s \lesssim 1$ to $n_s \approx 0.6$ reflects the pair-breaking effect of a significant concentration of non-magnetic impurities. Additional pair-breaking by dilute concentrations of paramagnetic impurities for n_s , and suppression of T_c , is also evident.

What is not visible in Fig. 9 are non-monotonic anomalies in $n_s(T, \omega)$ at very low temperature that are sensitive to the frequency of the microwave field. Figure 10 shows a non-monotonic variation of the superfluid fraction over a nar-

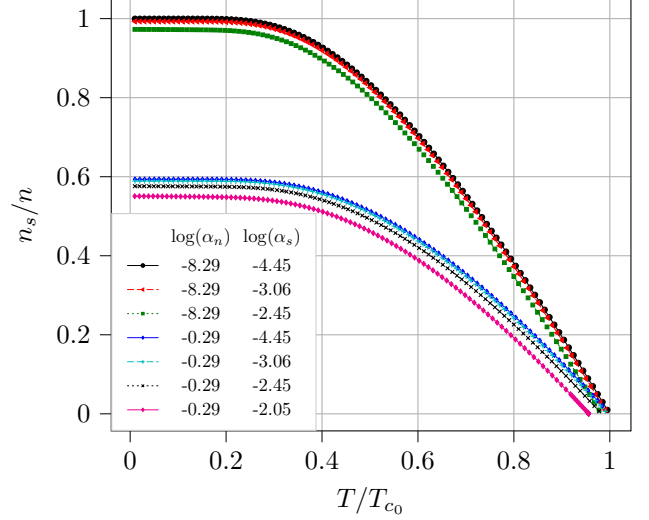


FIG. 9. The superfluid fraction, n_s/n , as a function of T/T_c for frequency $\omega = 0.005 T_{c0}$. Results are shown for low- and high-concentrations of non-magnetic impurities in the unitarity limit, $\alpha N = \Gamma_N/\pi T_{c0}$, and several low concentrations, $\alpha S = \Gamma_S/2\pi T_{c0}$, of paramagnetic impurities in the limit $\bar{u}_S = 1$.

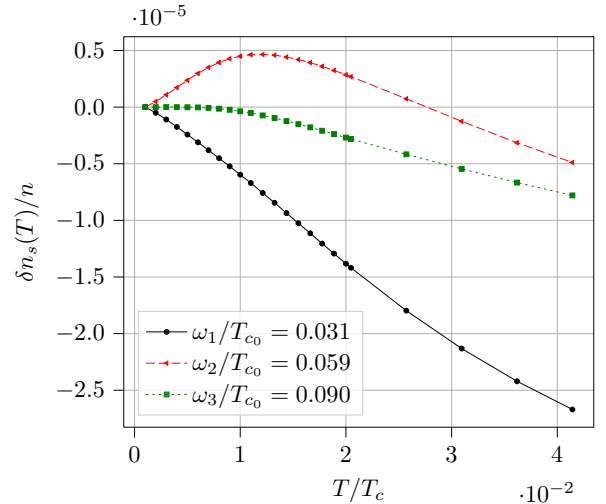


FIG. 10. Non-monotonic temperature and frequency dependence of the superfluid density for $0 < T \lesssim 0.04 T_c$, $\bar{u}_S = 0.975$, $\Gamma_S/2\pi T_{c0} = 8.9 \times 10^{-6}$ and microwave frequencies covering the position and bandwidth of the sub-gap quasiparticle band near the Fermi level as shown in Fig. 11.

row temperature range of order $0.04 T_c$, for three frequencies of the microwave field. Note that $\delta n_s/n$ is also a non-monotonic function of frequency in this temperature range. The magnitude of the non-monotonic variation is of order 5 ppm, which implies similar fractional changes in the penetration of the EM field into the surface of the superconductor,

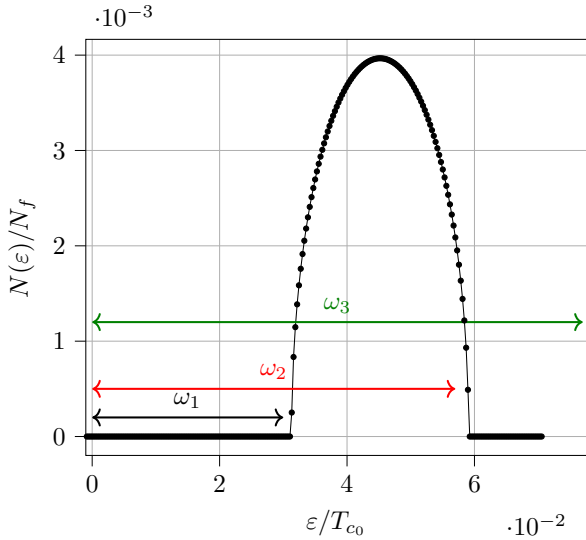


FIG. 11. The band of sub-gap quasiparticles near the Fermi level generated by a very dilute concentration, $\Gamma_S/2\pi T_c = 8.9 \times 10^{-6}$, of paramagnetic impurities with exchange interaction $\bar{u}_S = 0.975$. Also shown is the reach of microwave frequencies corresponding to the low-temperature superfluid response plotted in Fig. 10.

and thus to the resonant frequency of a superconducting resonators. These low-temperature, low-frequency anomalies in field penetration and resonant frequency originate from a low-concentration of sub-gap quasiparticle bands near, but not overlapping, the Fermi level, within reach of the microwave frequency as show in Fig. 11. The microwave field produces shifts in the occupation of the sub-gap quasiparticle bands above and below the Fermi level that contribute to the conductivity in Eq. (83). For frequency ω_2 shown in Fig. 11 that spans the positive energy sub-gap band the occupancy of the bands above and below the Fermi level are shifted to effectively suppress the thermal population of states above the Fermi level that would otherwise contribute to thermal backflow, and to increase the occupancy of the negative energy sub-gap band below the Fermi level, both leading to an initial increase in the superfluid fraction for $0 < T \lesssim 0.012 T_c$ as shown in Figure 10. The sensitivity of the superfluid response is also evident for the frequencies above and below ω_2 in Fig. 11.

High-Q superconducting resonators exhibit changes in their resonant frequency in the 1-10 ppm range [28]. Notable are Ta-based CPW resonators operating at 4.8 GHz exhibits a non-monotonic resonant frequency shift of order $\delta f/f \approx 0.5$ ppm at low temperatures as shown in Fig. 2b of Ref. 50. The authors attribute the anomaly to TLS defects. However, the non-monotonic anomaly we find at GHz frequencies results from the sub-gap quasiparticle response to the microwave field. Such states are excluded in the analysis of Ref. 50 because the authors assume Ta is a fully gapped superconductor.

C. Dissipative conductivity

In contrast to the non-dissipative response of the superfluid density, $n_s(T, \omega)$, the dissipative response, $\text{Re } \sigma(\omega, T)$, is sensitive to temperature, frequency, non-magnetic and paramagnetic impurity disorder, for all temperatures and frequencies, including very low-temperatures and microwave frequencies.

Fig. 12 shows the dissipative conductivity as a function of

temperature for the same parameters for non-magnetic and paramagnetic impurities as those in Fig. 9. A key observation is that a large coherence peak just below T_c results from a substantial concentration of non-magnetic impurity disorder, e.g. $\log(\Gamma_S/2\pi T_{c0}) = -0.29$, a value typical of high-Q niobium SRF cavities [14, 15, 37]. Another key observation is that for a fixed concentration of non-magnetic impurities *suppresses* the coherence peak. Thus, the sensitivity of the coherence peak could serve as a signature and measure of very dilute concentrations of paramagnetic impurities. What is not visible in Fig. 12 is the low temperature limit of the conductivity. We reveal this regime in Fig. 13; the logarithm highlights the saturation of $\text{Re } \sigma(\omega, T)$ below $T \approx 0.2 T_c$, for the same impurity parameters as those of Fig. 12. The limiting value of $\text{Re } \sigma$ for $T = 0$, which is determined by the dissipative response of the small, but finite, density of sub-gap quasiparticles at the Fermi level provides a physical mechanism for the residual resistance inferred from experimental measurements of the limiting Q of superconducting resonators [29]. We highlight these features of the microwave conductivity in the quality factor, Q , and resonance frequency shift, δf , of high-Q superconducting resonators.

D. Frequency shift, δf , and Q of cavity resonators

For transverse fields the current response expressed in terms of the conductivity, $\sigma(\omega)$, and electric field, $\mathbf{E}(\omega) = i\frac{\omega}{c}\mathbf{A}(\omega)$, is often expressed in terms of the response to the vector potential,

$$\mathbf{J}^R(\mathbf{q}, \omega) = -\frac{c}{4\pi} K(\omega) \mathbf{A}(\mathbf{q}, \omega). \quad (84)$$

The response function, $K(\omega, T)$, is related to the real and imaginary parts of the complex conductivity,

$$K(\omega, T) = \frac{1}{\lambda(\omega, T)^2} - i\frac{4\pi\omega}{c^2} \sigma_1(\omega, T), \quad (85)$$

where $\lambda(\omega, T)$ is the penetration depth of the EM field into the superconductor (Eq.(83)), and $\sigma_1 = \text{Re } \sigma(\omega, T)$ is the contribution to the conductivity that is in-phase with the electric field and thus determines the dissipation of the EM field by Joule losses from un-paired quasiparticles within the region of penetration of the EM field. For a fully gapped superconductor the Joule dissipation at microwave frequencies is exponentially suppressed at low temperatures leading to a diverging quality factor, $Q(\omega, T)$, for $T \rightarrow 0$. However, even a very small concentration of paramagnetic impurities with intermediate quasiparticle-impurity exchange interaction leads to dissipation by the microwave field at low temperatures from a band of sub-gap quasiparticles near the Fermi level, and thus a limiting value for Q , often interpreted in terms of a phenomenological ‘‘residual’’ surface resistance [51]. Below we show that a band of sub-gap states with a finite density of states at the Fermi level leads saturation of Q and a residual surface resistance for high-Q cavity resonators with very low concentrations of paramagnetic impurities.

The field, $\mathbf{A}(\mathbf{r}, \omega)$, and the current response, $\mathbf{J}^R(\mathbf{r}, \omega)$, in Eq. (84) are supplemented by boundary conditions for the vector potential at the vacuum-superconductor interface. The combination allow us to calculate the quality factor and resonant frequency shift of SRF cavities with high precision [14, 15].

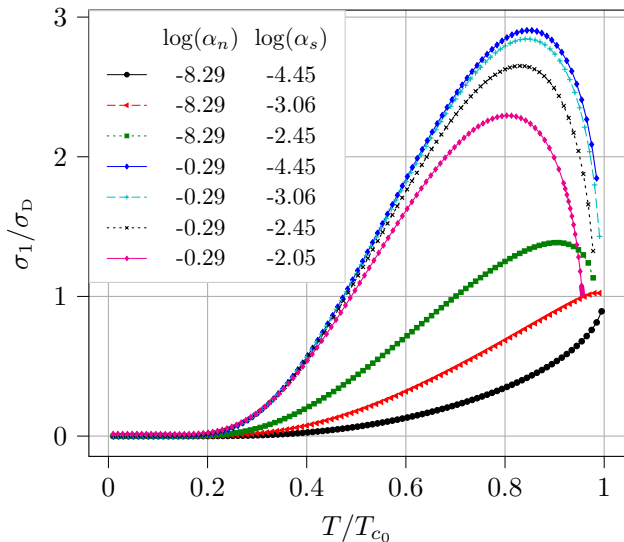


FIG. 12. The dissipative microwave conductivity, $\sigma_1(\omega, T)$, as a function of temperature for the same values of magnetic and non-magnetic impurities as those in Fig. 9, and $\omega = 0.005 T_c$. The conductivity is normalized to the normal-state Drude conductivity, $\sigma_D = \frac{ne^2\tau}{m^*}$, at T_c .

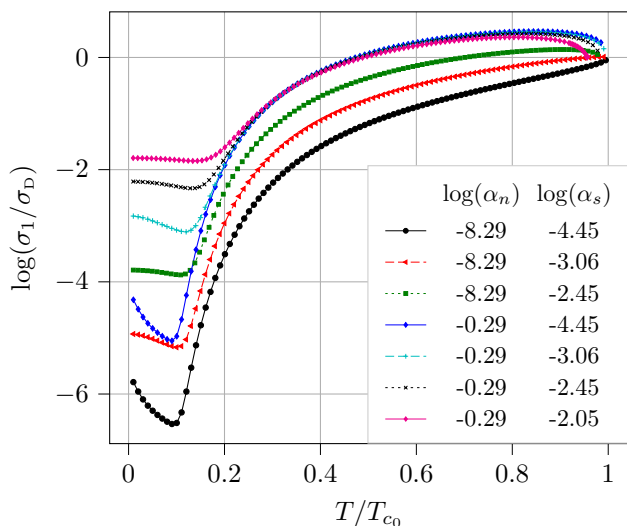


FIG. 13. The log of the dissipative conductivity, $\sigma_1(\omega, T)$, as a function of temperature for the same parameters as Fig. 12, which highlights the limiting value $\sigma_1(\omega)$ below a temperature of order the bandwidth of the sub-gap impurity band.

1. Quality factor of high-Q cavity resonators

The quality factor for the fundamental TM mode of a cylindrical SRF cavity at microwave frequencies is related to the current response function, $K(\omega, T)$, by

$$\frac{1}{Q} = \frac{2}{R} \text{Im} \left\{ \frac{1}{\sqrt{K}} \right\}, \quad (86)$$

where R is the radius of the cavity [15]. At microwave frequencies and low temperatures the penetration depth is finite while $\sigma_1(\omega, T)$ is decreasing exponentially with temperature down to very low temperatures as shown in Fig. 12. As a result the quality factor at low temperature is inversely pro-

portional to the dissipative conductivity,

$$Q(\omega, T) \approx \frac{R}{\lambda_\omega} \left(\frac{c^2}{4\pi\omega\lambda_\omega^2} \right) \frac{1}{\sigma_1(\omega, T)}, \quad T \ll T_c, \quad (87)$$

where $\lambda_\omega = \lambda(\omega, 0) \approx \lambda_L$, and ω is the resonant frequency of the SRF cavity. Thus, the low temperature behavior, including any zero-temperature limit, of Q is determined by the dissipative conductivity $\sigma_1(\omega, T)$ for $T \ll T_c$. In particular, for high-Q resonators with very low concentrations of paramagnetic impurities we predict a residual resistance $R_s(0) \propto \sigma_1(\omega, T=0)^{-1}$. The saturation and zero-temperature limit of Q at low temperatures is shown in Fig. 14 for several decades of very low concentrations of paramagnetic impurities [$\log(\alpha_s)$]. Note also that the saturation of Q is independent of the concentration of non-magnetic impurities for more than eight orders of magnitude. The maximum value of Q is exponentially sensitive to $\log(\alpha_s)$ as is evident in Fig. 14. It is also noteworthy that Q decreases as T drops below that corresponding to the maximum Q . This non-monotonic temperature dependence is qualitatively similar to what is observed in high-Q SRF cavities after the removal of surface oxides [29]. In our theory the non-monotonic temperature dependence is determined by the position (exchange energy) and width (concentration) of the sub-gap quasiparticle band at the Fermi level. It is worth noting that the saturation of Q at low temperature is not limited to pair-breaking by paramagnetic impurities. Embedded two-level tunneling impurities are also capable of creating a band of sub-gap states at the Fermi level, and thus a residual resistance and maximum Q for $T \ll T_c$ [7].

2. Resonant frequency shift of high-Q cavity resonators

The resonance frequency of a high-Q cavity generally increases by 1 – 10 ppm below T_c due to effective screening of the EM field compared to the normal metal skin depth. However, there is typically a negative frequency shift confined to a narrow temperature region near T_c that was highlighted in detailed measurements reported in Refs. [28, 52]. A quantitative theory of the small shifts in the resonant frequency of N-doped Nb high-Q resonators, including the negative frequency anomaly, was developed by Ueki et al. [14] and Zarea et al. [15]. These authors showed that the quality factor and frequency shift, including the observed temperature dependences, were quantitatively accounted for by the current response of Nb with non-magnetic disorder at levels of disorder below the clean to dirty limit cross-over, i.e. $0.5 \lesssim 1/2\pi\tau_N T_c \lesssim 0.75$ [14]. These authors also identified the mechanism responsible for the negative frequency shift in these resonators; as $\Delta T = T \rightarrow T_c$ from below the London penetration depth diverges and exceeds the normal metal skin depth, leading to a negative frequency shift within a temperature range of width $T_c - T \lesssim 4 \times 10^{-3} T_c$ near T_c [15]. Since these studies several groups have reported negative frequency shift anomalies in Nb-based SRF cavities, often with negative shift anomalies extending over a broader temperature range below T_c [53–55]. Here we report new theoretical results for the frequency shift of SRF cavity resonators with non-magnetic impurities and low concentrations of paramagnetic impurities.

The difference in the resonance frequency, $\delta f = f_s - f_0$, of a superconducting resonator, f_s , relative to the that of a perfect conductor f_0 is determined by the penetration of the EM field

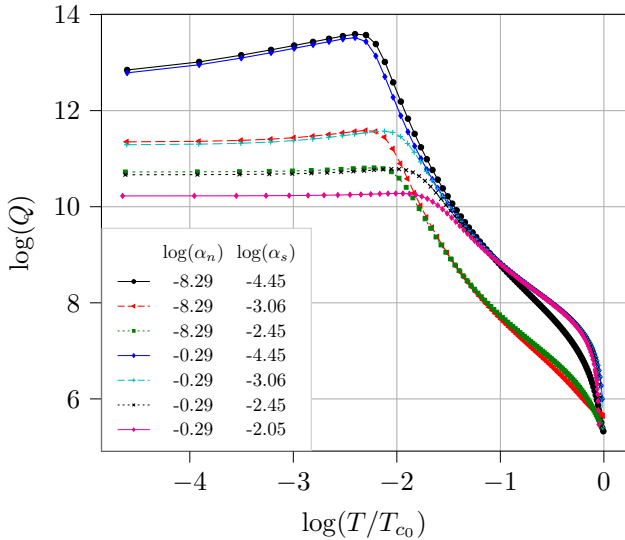


FIG. 14. Log-log plot of the quality factor as a function of temperature showing the maximum and zero-temperature limit for Q from a sub-gap band of quasiparticles for the same values of magnetic and non-magnetic impurities as those in Fig. 9.

into the superconductor, and given by

$$\frac{\delta f}{f} = -\frac{1}{R} \operatorname{Re} \left\{ \frac{1}{\sqrt{K}} \right\}. \quad (88)$$

Figure 15 shows the impact of paramagnetic impurity scattering on the frequency shift of superconducting resonators for temperatures in the vicinity of T_c for the clean limit for non-magnetic impurities and increasing concentrations of paramagnetic impurities.

An important parameter characterizing the frequency shift anomaly at high temperatures is the ratio of the normal-state electron-impurity scattering time, τ , to the period of the microwave field, $\omega\tau$, where $1/\tau = 1/\tau_N + 1/\bar{\tau}_{S_n}$. For $\omega\tau \approx 1$ the frequency shift at T_c , $\delta f|_{T_c}$, is the same order as the zero-temperature shift, $\delta f|_{T=0}$. The corresponding temperature width of the negative frequency shift region is of order, $\Delta T \approx 0.2T_c$, which is much wider than anomalous temperature region, $\Delta T \approx 4 \times 10^{-4}T_c$, for much higher concentrations of non-magnetic impurities characteristic of N-doped Nb SRF resonators [14, 15]. Indeed Fig. 16 shows results for $\omega\tau \ll 1$ associated with a concentration of non-magnetic impurities comparable to N-doped Nb SRF resonators.

Note (1) the narrow range of the negative frequency anomaly, $\Delta T \approx 6 \times 10^{-4}T_c$ and the maximum dip of $\delta f/f_0 \approx -0.5 \times 10^{-6}$, for the lowest concentration of paramagnetic impurities, $\log \alpha S = -4.45$, and (2) the substantial increase in both the width of the anomaly and the magnitude of the dip with increasing concentration of paramagnetic impurities.

What is significant here is that the width and magnitude of the negative frequency shift for $T \lesssim T_c$ are significant diagnostics of both non-magnetic and paramagnetic disorder in high-Q superconducting resonators.

IV. CONCLUSION

Optimizing the performance of superconducting resonators and devices requires identifying and eliminating sources of dissipation and decoherence, often embedded or interfacial

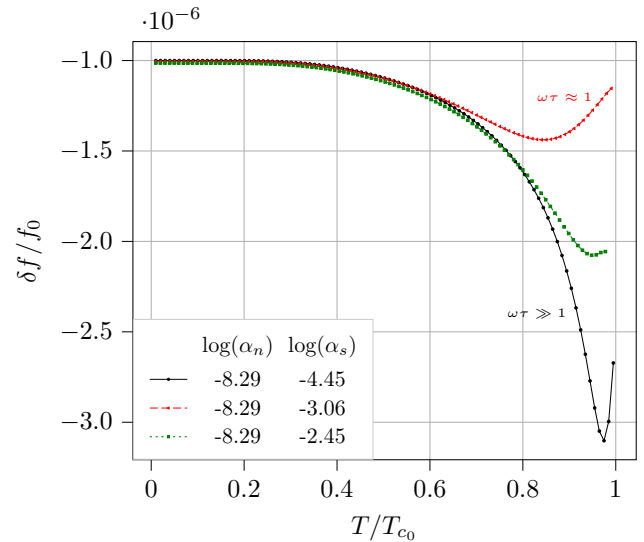


FIG. 15. The resonant frequency of a superconducting cavity resonator, relative to that for a perfect metal, as a function of temperature, for the nearly clean limit of non-magnetic disorder and a range of concentrations of non-magnetic impurities. The temperature width and magnitude of the negative frequency shift anomaly near T_c depends strongly on the ratio $\omega\tau$.

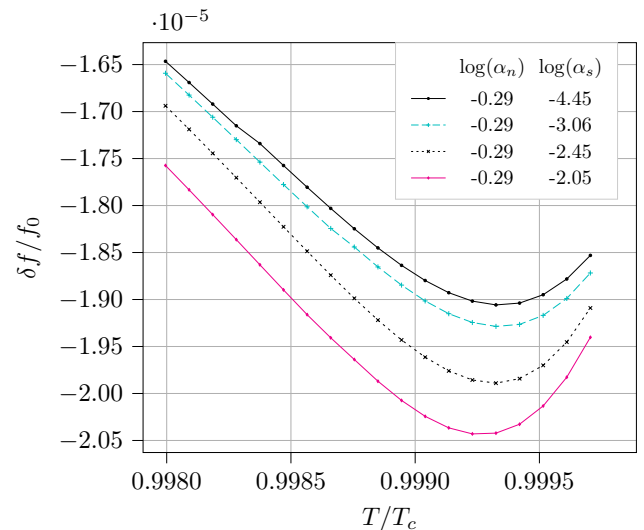


FIG. 16. The resonant frequency shift of an SRF resonator very near T_c for moderate non-magnetic disorder showing the effect for low concentrations of paramagnetic impurities.

defects, or two-level system defects. This task becomes more challenging as the performance level of the device increases.

We have shown that Joule dissipation from a sub-gap spectrum of un-paired quasiparticles, generated by dilute concentrations of paramagnetic impurities, limits the quality factor of superconducting resonators operating at microwave frequencies at low temperatures. In particular, a sub-gap band of quasiparticles overlapping the Fermi level provides a microscopic theory for the zero-temperature residual resistance of high-Q resonators. Signatures of non-magnetic and paramagnetic impurity disorder are observable in the temperature-dependent shifts of the resonant frequency of high-Q superconducting resonators.

V. ACKNOWLEDGEMENTS

We thank Maria Iavarone, Ruslan Prozorov and John Zasadinski for discussions and sharing their insights and evidence of sub-gap quasiparticles from STM, PCTS and London penetration depth measurements on superconducting niobium. The work of MZ was supported by the Hearne Institute of Theoretical Physics and the Center for Compu-

tational Technology at Louisiana State University. The work of JAS was supported by the U.S. Department of Energy, Office of Science, National Quantum Information Science Research Centers, Superconducting Quantum Materials and Systems Center (SQMS) under contract number DE-AC02-07CH11359.

-
- [1] K. Serniak, M. Hays, G. de Lange, S. Diamond, S. Shankar, L. D. Burkhardt, L. Frunzio, M. Houzet, and M. H. Devoret. Hot Nonequilibrium Quasiparticles in Transmon Qubits. *Phys. Rev. Lett.*, 121:157701, 2018. doi: 10.1103/PhysRevLett.121.157701.
- [2] P. J. de Visser, D. J. Goldie, P. Diener, S. Withington, J. J. A. Baselmans, and T. M. Klapwijk. Evidence of a Nonequilibrium Distribution of Quasiparticles in the Microwave Response of a Superconducting Aluminum Resonator. *Phys. Rev. Lett.*, 112:047004, 2014. doi: 10.1103/PhysRevLett.112.047004.
- [3] S. Chowdhury, M. Hays, S. R. Jha, K. Serniak, T. P. Orlando, J. A. Grover, and W. D. Oliver. Theory of Quasiparticle Generation by Microwave Drives in Superconducting Qubits. *arXiv*, page 2505.00773, 2025. doi: 10.48550/arXiv.2505.00773.
- [4] L. Cardani and et al. Reducing the impact of radioactivity on quantum circuits in a deep-underground facility. *Nature Communications*, 12(1):2733, 2021. doi:10.1038/s41467-021-23032-z.
- [5] L. Cardani, I. Colantoni, A. Cruciani, and et al. Disentangling the sources of ionizing radiation in superconducting qubits. *The European Physical Journal C*, 83(1):94, 2023. doi:10.1140/epjc/s10052-023-11199-2.
- [6] S. E. de Graaf and et al. Two-level systems in superconducting quantum devices due to trapped quasiparticles. *Science Advances*, 6(51):eabc5055, 2020. doi:10.1126/sciadv.abc5055.
- [7] J. He, W.-T. Lin, and J. A. Sauls. Theory of Two-Level Tunneling Systems in Superconductors. *Prog. Theor. Exp. Phys.*, 2025:063101, 2025. doi:10.1093/ptep/ptaf081.
- [8] J. Bardeen, L. Cooper, and J. Schrieffer. Theory of Superconductivity. *Phys. Rev.*, 108(5):1175–1204, 1957. doi: 10.1103/PhysRev.108.1175.
- [9] P. W. Anderson. Theory of Dirty Superconductors. *J. Phys. Chem. Sol.*, 11(1–2):26 – 30, 1959. doi:10.1016/0022-3697(59)90036-8.
- [10] A. A. Abrikosov and L. P. Gorkov. Superconducting Alloys at Finite Temperatures. *JETP*, 9:220, 1959. URL <http://jetp.ras.ru/cgi-bin/e/index/e/9/1/p220?a=list>.
- [11] A. A. Abrikosov and L. P. Gorkov. Contribution to the Theory of Superconducting Alloys with Paramagnetic Impurities. *JETP*, 12:1243, 1961.
- [12] K. Maki. On Persistent Currents in a Superconducting Alloy. I. *Prog. Theor. Phys.*, 29:10–22, 1963. doi: 10.1143/PTP.29.10.
- [13] J. A. Sauls. Theory of disordered superconductors with applications to nonlinear current response. *Prog. Theor. Exp. Phys.*, 2022(3), 02 2022. ISSN 2050-3911. doi: 10.1093/ptep/ptac034. 033103.
- [14] H. Ueki, M. Zarea, and J. A. Sauls. The Frequency Shift and Q of Disordered Superconducting RF Cavities. *Prog. Theor. Exp. Phys.*, 2025:053102, 2025. doi:10.1093/ptep/ptaf061.
- [15] M. Zarea, H. Ueki, and J. A. Sauls. Electromagnetic Response of Disordered Superconducting Cavities. *Frontiers in Superconducting Materials*, 3:1–7, 2023. doi: 10.3389/femat.2023.1259401. Special Issue: Progress on Superconducting Materials for SRF Applications.
- [16] H. Ueki and J. A. Sauls. Photon Frequency Conversion in High-Q Superconducting Resonators: Axion Electrodynamics, QED and Nonlinear Meissner Radiation. *Prog. Theor. Exp. Phys.*, 2024:123101, 2024. doi:10.1093/ptep/ptae183.
- [17] A. Lebedeva, M. Hladký, M. Polák, and F. Herman. Local-limit disorder characteristics of niobium-based superconducting radio-frequency cavities. *Phys. Rev. Appl.*, 24(4):044007, 2025. doi:10.1103/5hp2-3x8n.
- [18] K. Maki. *Superconductivity*, volume II, chapter 18, page 1035. Marcel Dekker Inc., 1st edition, 1969.
- [19] L. Yu. Bound State in Superconductors with Paramagnetic Impurities. *Acta Physica Sinica*, 21(1):75, 1965. doi: 10.7498/aps.21.75.
- [20] H. Shiba. Classical Spins in Superconductors. *Progress of Theoretical Physics*, 40(3):435–451, 1968. doi: 10.1143/PTP.40.435.
- [21] A. I. Rusinov. Superconductivity near a Paramagnetic Impurity. *JETP Lett.*, 9:146, 1969. URL http://jetpletters.ru/ps/0/article_25295.shtml.
- [22] K. Machida and F. Shibata. Bound States Due to Resonance Scattering in Superconductor. *Prog. Theor. Phys.*, 47(6):1817–1823, 1972. doi:10.1143/PTP.47.1817.
- [23] G. Eilenberger. Transformation of Gorkov’s Equation for Type II Superconductors into Transport-Like Equations. *Zeit. f. Physik*, 214:195, 1968. doi:10.1007/BF01379803.
- [24] A. I. Larkin and Y. N. Ovchinnikov. Quasiclassical Method in the Theory of Superconductivity. *JETP*, 28:1200–1205, 1969.
- [25] G. M. Eliashberg. Inelastic electron collisions and nonequilibrium stationary states in superconductors. *JETP*, 34:668, 1972.
- [26] S. F. Edwards. A New Method for the Evaluation of the Electrical Conductivity in Metals. *Phil. Mag.*, 3:1020, 1958. doi: 10.1080/14786435808243244.
- [27] D. Rainer and J. A. Sauls. *Strong-Coupling Theory of Superconductivity*, volume 1809.05264, pages 1–24. 2018. URL <https://arxiv.org/abs/1809.05264>. Published in “Superconductivity: From Basic Physics to New Developments”, ch. 2, pp. 45–78, World Scientific, Singapore (1994).
- [28] D. Bafia, A. Grassellino, M. Checchin, J. F. Zasadzinski, and A. Romanenko. Signatures of enhanced superconducting properties in niobium cavities. *Phys. Rev. Appl.*, 23:054052, 2025. doi:10.1103/PhysRevApplied.23.054052.
- [29] A. Romanenko, R. Pilipenko, S. Zorzetti, D. Frolov, M. Awida, S. Belomestnykh, S. Posen, and A. Grassellino. Three-Dimensional Superconducting Resonators at $T < 20$ mK with Photon Lifetimes up to $T_1 = 2$ s. *Phys. Rev. Applied*, 13:034032, 2020. doi:10.1103/PhysRevApplied.13.034032.
- [30] A. Abrikosov, L. Gorkov, and I. Dzyaloshinski. *Methods of Quantum Field Theory in Statistical Physics*. Prentice-Hall, Inc., Englewood Cliffs, NJ, 1963.
- [31] J. R. Schrieffer. *The Theory of Superconductivity*. Addison-Wesley Publishing Company, New York, 1964.
- [32] L. P. Gorkov. On the Energy Spectrum on Superconductors. *JETP*, 7(3):505–508, 1958. URL <http://jetp.ras.ru/cgi-bin/e/index/e/7/3/p505?a=list>. Russian: ZhETF, 34, 3, 735 (1958).
- [33] H. Ueki, M. Zarea, and J. A. Sauls. The Frequency Shift and Q of Disordered Superconducting RF Cavities. *arXiv*, 2207.14236:1–11, 2022. doi:10.48550/arXiv.2207.14236.
- [34] W. Lee, D. Rainer, and W. Zimmermann. Holstein Effect in the Far-Infrared Conductivity of High T_c Superconduc-

- tors. *Physica C*, 159(5):535–544, 1989. doi:10.1016/0921-4534(89)91284-7.
- [35] O. Shevtsov and J. A. Sauls. Electrons and Weyl Fermions in Superfluid $^3\text{He-A}$. *Phys. Rev. B*, 94:064511, 2016. doi:10.1103/PhysRevB.94.064511.
- [36] N. F. Mott and H. Jones. *The Theory of the Properties of Metals and Alloys*. Dover Publications, New York, 1958.
- [37] M. Zarea, H. Ueki, and J. A. Sauls. Effects of Anisotropy and Disorder on the Superconducting Properties of Niobium. *Frontiers in Physics*, 11:1269872, 2023. doi:10.3389/fphy.2023.1269872.
- [38] D. Xu, S. K. Yip, and J. A. Sauls. Nonlinear Meissner Effect in Unconventional Superconductors. *Phys. Rev. B*, 51:16233, 1995. doi:10.1103/PhysRevB.51.16233.
- [39] A. Sakurai. Comments on Superconductors with Magnetic Impurities. *Prog. Theor. Phys.*, 44(6):1472–1476, 1970. doi:10.1143/PTP.44.1472.
- [40] M. I. Salkola, A. V. Balatsky, and J. R. Schrieffer. Spectral properties of quasiparticle excitations induced by magnetic moments in superconductors. *Phys. Rev. B*, 55(18):12648–12661, 1997. doi:10.1103/PhysRevB.55.12648.
- [41] M. Abramowitz and I. Stegun. *Handbook of Mathematical Functions*. U.S. Government Printing Office, Washington D.C., tenth printing edition, 1972.
- [42] V. Ambegaokar and A. Griffin. Theory of the Thermal Conductivity of Superconducting Alloys with Paramagnetic Impurities. *Phys. Rev.*, 137(4A):A1151–A1167, 1965. doi:10.1103/PhysRev.137.A1151.
- [43] S. Ali, L. Zhang, and J. A. Sauls. Thermodynamic Potential for Superfluid ^3He in Silica Aerogel. *J. Low Temp. Phys.*, 162(3-4):233–242, 2011. doi:10.1007/s10909-010-0310-4.
- [44] M. J. Graf, S.-K. Yip, J. A. Sauls, and D. Rainer. Electronic Thermal Conductivity and the Wiedemann-Franz Law for Unconventional Superconductors. *Phys. Rev. B*, 53:15147, 1996. doi:10.1103/PhysRevB.53.15147.
- [45] J. A. Sauls and T. Mizushima. On the Nambu Fermion-Boson Relations for Superfluid ^3He . *Phys. Rev. B*, 95:094515, 2017. doi:10.1103/PhysRevB.95.094515.
- [46] J. A. Sauls. Quasiclassical Linear Response Theory á la Matsubara and Eliashberg. 2025.
- [47] G. M. Eliashberg. *JETP*, 34:668, 1972. [zetf, 61, 1254 (1971)].
- [48] D. C. Mattis and J. Bardeen. Theory of the Anomalous Skin Effect in Normal and Superconducting Metals. *Phys. Rev.*, 111:412–417, 1958. doi:10.1103/PhysRev.111.412.
- [49] A. Abrikosov, L. P. Gorkov, and I. M. Khatlatnikov. A Superconductor in a High Frequency Field. *JETP*, 35(1):182–189, 1959.
- [50] K. D. Crowley, R. A. McLellan, A. Dutta, and et al. Disentangling Losses in Tantalum Superconducting Circuits. *Phys. Rev. X*, 13:041005, 2023. doi:10.1103/PhysRevX.13.041005.
- [51] A. Romanenko, C. J. Edwardson, P. G. Coleman, and P. J. Simpson. The effect of vacancies on the microwave surface resistance of niobium revealed by positron annihilation spectroscopy. *Applied Physics Letters*, 102:232601, 2013. doi:10.1063/1.4811090.
- [52] D. Bafia, A. Grassellino, M. Checchin, J. Zasadzinski, and A. Romanenko. The Anomalous Resonant Frequency Variation of Microwave Superconducting Niobium Cavities Near T_c . *arXiv*, 2103.10601, 2021. doi:10.48550/arXiv.2103.10601.
- [53] H. Ito. *High-Q performance of SRF cavities by mid-T baking at KEK*. 2021. URL https://indico.desy.de/event/27572/contributions/94297/attachments/63541/77668/TTC2021_Ito.pdf.
- [54] R. Ghanbari, C. Bate, G. Deyu, W. Hillert, R. Monroy-Villa, D. Reschke, L. Steder, M. Wenskat, and J. Wolff. Correlating Lambda Shift Measurements with RF Performance in Mid-T Heat Treated Cavities. In *Proceedings of SRF2023*, pages 124–128. JACOW Publishing, Geneva, Switzerland, 2023. ISBN 978-3-95450-234-9. doi:10.18429/JACoW-SRF2023-MOPMB021.
- [55] Dhakal,Pashupati, Khanal,Bashu, Lechner,Eric, and Ciovati,Gianluigi. Impact of medium temperature heat treatment on flux trapping sensitivity in SRF cavities. In *Proceedings of IPAC'24 - Nashville, TN*, pages 2764–2767. JACoW Publishing, 2024. ISBN 9783954502479. doi:10.18429/JACOW-IPAC2024-WEPS33.